Title: Optimized CART Cell Therapy for Metastatic Aggressive Thyroid Cancer

Authors: Claudia Manriquez Roman[1,2,3†], Elizabeth L. Siegler[2,3†], Justyna J. Gleba[4†], Truc N. Huynh[2,3], Grace E. DeFranco[2,5,6], Aylin Alasonyalilar Demirer[4], Matthew L. Pawlush[4], Michael Redig[4], Skyeler M. Klinge[4], Long K. Mai[2,3], , James L. Miller[4], Erin E. Miller[4], Brooke L. Kimball[2,3], Erin E. Tapper[2,3], R. Leo Sakemura[2,3], Carli M. Stewart[2,6,7], Ismail Can[2,3], Olivia L. Sirpilla[2,3], Jennifer M. Feigin[2,6,8], Kun Yun[2,6,9], Omar L. Gutierrez Ruiz[2,3], Hong Xia[2,3], Mehrdad Hefazi Torghabeh[2,3], Kendall J. Schick[2], Ekene J. Ogbodo[2,3], Gloria Olivier[10], Yushi Qiu[4], Robert C. Smallridge[11], Abba Zubair[12], Han W. Tun[13], John A. Copland[4,8,9*], and Saad S. Kenderian[1,2,3,5,6,9*]

Affiliations:
[1] Center for Regenerative Biotherapeutics, Mayo Clinic; Rochester, MN
[2] T Cell Engineering Laboratory, Mayo Clinic; Rochester, MN
[3] Division of Hematology, Mayo Clinic; Rochester, MN
[4] Cancer Biology Department, Mayo Clinic; Jacksonville, FL
[5] Department of Immunology, Mayo Clinic; Rochester, MN
[6] Mayo Clinic Graduate School of Biomedical Sciences; Rochester, MN
[7] Department of Molecular Pharmacology and Experimental Therapeutics, Mayo Clinic; Rochester, MN
[8] Department of Biochemistry and Molecular Biology, Mayo Clinic; Rochester, MN
[9] Department of Molecular Medicine, Mayo Clinic; Rochester, MN
[10] Department of Business Development, Mayo Clinic; Rochester, MN
[11] Division of Endocrinology, Internal Medicine Department, Mayo Clinic; Jacksonville, FL
[12] Department of Laboratory Medicine and Pathology, Mayo Clinic; Jacksonville FL
[13] Hematology/Oncology Division, Department of Medicine, Mayo Clinic; Jacksonville, FL

† These authors contributed equally to this work

* Corresponding authors: Saad S. Kenderian, Mayo Clinic Rochester, 200 First Street S.W., Rochester, MN Kenderian.saad@mayo.edu, *or* John A. Copland, Mayo Clinic Florida, copland.john@mayo.edu

Running Title: TSHR-CART cell therapy in thyroid cancers

Acknowledgements: This study was partly funded through the following:
Mayo Clinic Center for Regenerative Biotherapeutics (JAC and SSK)
Mayo Clinic Comprehensive Cancer Center (SSK)
National Institutes of Health R37CA266344 and R01AI79974 (SSK)
Department of Defense grant CA201127 (SSK)
Generous support from Renee Cousins King, M.D.

Competing Interests: SSK is an inventor on patents in the field of CAR immunotherapy that are licensed to Novartis (through an agreement between Mayo Clinic, University of Pennsylvania, and Novartis). SSK and RLS are inventors on patents that are licensed to Humanigen/Taran (through Mayo Clinic). SSK is an inventor on patents that are licensed to MustangBio (through Mayo Clinic). ELS, EET, RLS, OLS, KJS, and SSK are inventors on patents that are licensed to Chymal (through Mayo Clinic). CMR, ELS, TNH, LKM, BLK, RLS, CMS, IC, OLS, JMF, KY, OGR, HX, MHT, JAC and SSK are inventors on patents licensed to Immix (through Mayo Clinic). SSK receives research funding from Kite, Gilead, Juno, BMS, Novartis, Humanigen/Taran, MorphoSys, Tolero, Sunesis/Viracta, LifEngine Animal Health Laboratories Inc, and Lentigen. SSK has participated in advisory meetings with Kite/Gilead, Calibr, Luminary Therapeutics, Humanigen, Juno/BMS, Capstan Bio, Carisma, and Novartis. SSK has served on the data safety and monitoring board with Humanigen. SSK has served as a consultant for Torque, Calibr, Novartis, Capstan Bio, and Humanigen

56 **ABSTRACT**

57 Most thyroid cancer deaths are attributed to a subset of poorly differentiated, metastatic tumors.
58 To improve treatment options for aggressive thyroid cancers, we developed a novel thyroid-
59 stimulating hormone receptor (TSHR)-targeted chimeric antigen receptor T (CART) cell therapy,
60 which demonstrated antigen-specific activation and antitumor efficacy against $TSHR^+$ cell lines *in*
61 *vitro* and *in vivo*. However, de-differentiated thyroid cancers downregulate TSHR. We therefore
62 developed a potent treatment strategy by combining our novel TSHR-CART cells with mitogen-
63 activated protein kinase (MAPK) inhibitors, which redifferentiate thyroid tumors and upregulate
64 TSHR expression. In patient-derived anaplastic thyroid cancer xenografts, combination therapy
65 of TSHR-CART cells and MAPK inhibitors led to increased TSHR expression on the tumor tissue
66 and significantly enhanced antitumor efficacy and prolonged survival compared to TSHR-CART
67 monotherapy. Based on our data, we are launching a phase I clinical trial for TSHR-CART cell
68 therapy alone or in combination with MAPK inhibitors in patients with metastatic thyroid cancers.

69

70 **STATEMENT OF SIGNIFICANCE**

71 Poor target selection and antigen escape limit CART cell efficacy in solid tumors. We developed
72 TSHR-CART cells to treat differentiated thyroid cancers but observed TSHR downregulation in
73 dedifferentiated thyroid cancers. We found that MAPK inhibitors restored TSHR expression and
74 sensitized these cancers to TSHR-CART cell therapy.

75

INTRODUCTION

Thyroid cancer is the most common endocrine cancer, and its incidence is rising in the US and globally.(*1, 2*) Thyroid cancer is projected to become the fourth leading type of cancer across the world, and the causes appear to be complex and multifactorial, including dietary changes and environmental exposures. Patients with thyroid cancer have widely different clinical outcomes depending on the pathological subtype and mutation profile. Metastatic differentiated thyroid cancer (DTC), poorly differentiated thyroid cancer (PDTC), and anaplastic thyroid cancer (ATC) account for a majority of thyroid cancer-related deaths, even though these subtypes only represent 2-3% of all thyroid cancer diagnoses.(*1, 3, 4*) Hurthle cell carcinoma (HCC, now termed oncocytic thyroid cancer(*5*)) is a subtype of DTC known to be aggressive, highly metastatic, and have lower rates of overall survival than follicular thyroid cancers. HCC is often resistant to radioiodine therapy and has no current FDA-approved treatment options.(*6, 7*) PDTC and ATC are aggressive and often refractory to radioiodine therapy and other standard therapies.(*8, 9*) SEER database analysis through 2015 reported a median overall survival of 4 months in patients with ATC, with disease-specific mortality of over 98%. A more recent analysis reported a median overall survival of 15.7 months in patients with ATC receiving newer targeted therapies.(*10*) Despite these advancements in treatment options, PDTC and ATC remain incredibly lethal.

Chimeric antigen receptor (CAR) T cell therapy has emerged as a potentially curative therapy in a subset of patients with hematological malignancies and has been FDA-approved for several B cell malignancies as well as for multiple myeloma.(*11-15*) With the advent of adoptively transferred engineered cellular therapies, there is a compelling rationale to apply CART cell therapy to treatment-resistant solid tumors. To date, the efficacy of CART cell therapy in solid tumors has been modest at best.(*16-21*) Due to a lack of tumor-specific targets for CART cell therapy in solid tumors, identifying an antigen that is both uniquely and universally expressed on cancer cells is critical for development of antigen-specific immunotherapy to avoid on-target off-tumor toxicities.(*20, 22, 23*)

102 Thyroid-stimulating hormone receptor (TSHR) is a surface glycoprotein receptor and a major
103 regulator of thyroid function and metabolism. The TSHR mediates the activating mechanism of
104 TSH to the thyroid gland, resulting in the growth and proliferation of thyrocytes as well as thyroid
105 hormone production, including thyroxine (T4) and triiodothyronine (T3).(*24*) TSHR is
106 predominantly expressed on the basolateral membrane of normal thyroid follicular cells.(*25*)
107 TSHR expression is largely limited to the thyroid gland, with low levels of expression in additional
108 tissues, including the thymus and testes (immune privileged) according to Human Protein Atlas
109 and NIH GenBank databases. TSHR is abundantly expressed on thyroid tumor cells.(*25, 26*)
110 Given its unique expression, TSHR is recognized as a compelling target for advanced thyroid
111 cancer diagnostics and therapy after thyroidectomy. Overall, there is limited risk of off-tumor
112 adverse effects of targeting TSHR. TSHR has been targeted using biologics including monoclonal
113 antibodies for the treatment of Graves' disease and thyroid cancer.(*27*) In this study, we
114 generated CART cells targeting TSHR (TSHR-CART) and showed potent, antigen-specific
115 antitumor efficacy against TSHR-expressing cell lines *in vitro* and *in vivo,* as well as in patient-
116 derived xenograft (PDX) mouse models of ATC.
117 Further, we identified mitogen-activated protein kinase (MAPK) inhibition as a strategy to
118 upregulate TSHR in dedifferentiated thyroid cancers and increase the therapeutic index of TSHR-
119 CART cell therapy. Downregulation of TSHR expression in dedifferentiated thyroid cancer is a
120 potential mechanism of resistance to TSHR-CART cell therapy. MAPK inhibition is an FDA-
121 approved treatment against thyroid cancer and is documented to upregulate TSHR expression in
122 patients with advanced metastatic thyroid cancer.(*28, 29*) Clinical trials for metastatic thyroid
123 cancers have demonstrated that MAPK inhibition induces re-expression of genes necessary for
124 iodine uptake and retention, including TSHR and sodium iodide symporter (NIS).(*30, 31*)
125 Additionally, many thyroid cancers have gene mutations involving the constitutive activation of
126 BRAF, which stimulates MAPK signaling.(*32-34*) Therefore, when BRAF activation is switched
127 off genetically, or its downstream signaling is inhibited with MEK inhibitors (MEKi) or BRAF

128 inhibitors (BRAFi), tumors re-express TSHR and NIS and reaccumulate iodine. This strategy has
129 been employed in the clinic to enhance the response to radioactive iodine therapy.(*29*)
130 We therefore sought to address antigen escape in ATC by testing the combination of MEK/BRAF
131 small molecule inhibitors with TSHR-CART cell therapy. We found that MEK/BRAF inhibition led
132 to restoration of TSHR expression on thyroid cancer cells and enhancement of CART cell
133 expansion and antitumor activity *in vivo*. This strategy is highly translatable to patients with
134 advanced thyroid cancers who have extremely limited treatment options to date.
135

136 **RESULTS**

137 **TSHR as a target for CART cell therapy**

138 To validate TSHR as a target candidate for CART cell therapy in thyroid cancer, we verified its
139 expression on thyroid tissue and lack of expression on other normal tissues by
140 immunohistochemistry (IHC) analysis of specimens from the Mayo Clinic Thyroid Cancer Biobank
141 and on publicly available databases.(*35*) IHC analysis showed that, while TSHR expression was
142 high in normal thyroid tissue as well as multiple thyroid cancer histotypes, ATC samples
143 demonstrated attenuated TSHR expression (**Fig. 1A, B**). We then assessed TSHR expression in
144 a healthy tissue microarray and confirmed that TSHR expression was high in the thyroid and low
145 or absent in other tissues including adult thymus and testis (**Fig. 1C, Supplementary Fig. S1**).
146 Having validated TSHR as a potential antigen to target with CART cell therapy, we designed and
147 generated TSHR-CART cells using a single chain variable fragment isolated from the TSHR
148 autoantibody clone K1-70 and cloned into a lentiviral CAR construct containing 4-1BB and CD3ζ
149 (**Supplementary Fig. S2A**). Healthy donor T cells transduced with CAR-encoded lentiviral
150 particles (**Supplementary Fig. S2B**) demonstrated high CAR expression as assessed by flow
151 cytometry (**Fig. 1D**). TSHR-CART cells displayed comparable CD4:CD8 ratio and phenotype
152 compared to control untransduced T cells (UTD) (**Supplementary Fig. S2C-D**).

153 **TSHR-CART cells exhibit potent and specific antitumor activity *in vitro***

154 We next examined the antigen-specific activation of TSHR-CART cells *in vitro* and *in vivo*. TSHR-
155 CART cells or UTD were incubated with the follicular thyroid cancer cell line, FTC-133, which was
156 transduced to overexpress TSHR; TSHR was transduced in these cells as thyroid cancer cell
157 lines and patient samples downregulate TSHR expression after extended monolayer cell
158 culture.(*36-39*) While TSHR-CART cells were not activated against wildtype ($TSHR^-$) FTC-133
159 cells, TSHR-CART cells demonstrated profound antigen-specific effector functions against
160 $TSHR^+$ target cells *in vitro*, including cytotoxicity against target cells (**Fig. 1E**) as well as TSHR-
161 CART proliferation (**Fig. 1F-G, Supplementary Fig. S3A**), degranulation (**Fig. 1H**), and cytokine
162 production (**Fig. 1I-L**). Similar results were found for wildtype ($TSHR^-$) and $TSHR^+$ THJ-529, a
163 PDTC cell line (**Supplementary Fig. S3B-H**).

164 **TSHR-CART cells show durable antitumor activity in xenograft HCC models**

165 We then assessed TSHR-CART cell activity in a xenograft model of HCC. We first measured
166 TSHR expression via IHC on biopsies obtained from patients with normal thyroid tissue, primary
167 HCC with minimal or extensive invasion, locally recurrent HCC, and metastatic HCC. Strong
168 TSHR expression was maintained in recurrent and metastatic lesions as well as primary tumors
169 (**Fig. 2A-B**). Having verified that HCC retains TSHR expression in patient samples and thus
170 providing a strong rationale for the use of TSHR-CART cell monotherapy, we then assessed the
171 *in vivo* activity of TSHR-CART cells against the $TSHR^+$ HCC cell line, XCT.UC1 as a proof of
172 concept. Non-obese diabetic severe combined immunodeficiency $IL2r\gamma^-/^-$ (NSG) mice were
173 subcutaneously engrafted with 1 x 10^7 XTC.UC1, which retains high endogenous TSHR
174 expression *in vivo*, and treated with 1 x10^7 UTD or TSHR-CART cells when tumors reached
175 ~100mm^3. Mice in remission were rechallenged with 1 x 10^7 XTC.UC1 cells subcutaneously in
176 the opposite flank (**Fig. 2C**). Serial caliper measurements revealed significant antitumor efficacy
177 of TSHR-CART cells compared to UTD control; by Day 50 post-engraftment, all UTD-treated mice
178 had reached humane endpoints, while all TSHR-CART-treated mice were in remission or had

179 small tumors (**Fig. 2D-E**). TSHR-CART-treated mice in remission were then rechallenged on Day
180 51 with XTC.UC1 in the opposite flank and were followed for tumor growth along with a new group
181 of untreated XTC.UC1-bearing mice as controls. Again, TSHR-CART cells displayed potent
182 antitumor activity; both original and rechallenged tumors were significantly suppressed compared
183 to untreated controls (**Fig. 2F**). Peripheral blood sampling at 21 days post-tumor rechallenge
184 revealed significantly higher numbers of human $CD3^+$ T cells in TSHR-CART-treated mice
185 compared to controls (**Fig. 2G**). These data demonstrated that TSHR-CART cells exerted durable
186 tumor control in HCC, an aggressive disease setting with no current standard of care.

187 **TSHR-CART cells demonstrate strong antitumor effects in $TSHR^+$ PDX models of PDTC**

188 Next, we evaluated the antitumor activity of TSHR-CART cells in a dose escalation model in NSG
189 mice. Here, we utilized aggressive, BRAF-mutant, patient-derived PDTC cells, THJ-529T, which
190 were transduced to overexpress TSHR. Mice were subcutaneously injected with 2.5 x 10^6
191 THJ-529T cells, and engraftment was confirmed by caliper measurement of tumor masses. When
192 tumors reached ~100mm^3, mice were randomized to treatment with 5 x 10^6 UTD, 5 x 10^6 TSHR-
193 CART cells, or 1 x 10^7 TSHR-CART cells (**Fig. 3A**). Treatment with TSHR-CART cells led to
194 significant and dose-dependent tumor control (**Fig. 3B-E, Supplemental Fig. S4A-C**), improved
195 survival outcomes (**Fig. 3F, Supplemental Fig. S4D**), increased tumor-infiltrated human T cells
196 (**Fig. 3G-H**), and increased human T cell proliferation in the peripheral blood (**Supplemental Fig.**
197 **S4E**). Having shown that the 1 x 10^7 TSHR-CART dose yielded superior antitumor activity
198 compared to the 5 x 10^6 TSHR-CART dose, we did not further pursue testing of the 5 x 10^6 TSHR-
199 CART dose.

200 **TSHR is downregulated in ATC but is restored with MAPK inhibition**

201 ATC cells have been associated with de-differentiation and downregulation of TSHR expression,
202 and we showed that ATC significantly downregulated TSHR expression compared to normal
203 thyroid tissues or more differentiated thyroid cancers (**Fig. 1A, B**). This observed downregulation

204 raises concerns for antigen escape and subsequent resistance to TSHR-CART cell therapy. We
205 first verified that the MEKi, trametinib, restored TSHR expression in an ATC PDX proof-of-concept
206 model. In this model, 5mm^3 Th-560 ATC PDX tissue was surgically implanted subcutaneously in
207 NSG mice. When tumors reached approximately 100mm^3, mice were randomized to daily
208 treatment with either vehicle control or MAPK inhibitors at the indicated doses until the
209 experimental endpoint (**Fig. 4A**). The administration of MEKi (trametinib) resulted in significant
210 dose-dependent slowing of tumor growth (**Fig. 4B**) as well as TSHR re-expression which inversely
211 correlated with pERK expression (**Fig. 4C**) after one week of daily trametinib treatment compared
212 to placebo treatment. Because many ATC tumors are BRAF-mutant, we performed a similar
213 experiment in which mice received either vehicle control or the dual MEKi/BRAFi R05126766 at
214 the indicated doses. Treatment with R05126766 resulted in a significant dose-dependent slowing
215 of tumor growth (**Fig. 4D**), and pERK expression inversely correlated with TSHR expression (**Fig.
216 4E**) after one week of daily R05126766 treatment compared to placebo treatment. Similarly,
217 treatment with combination of MEKi (trametinib) and BRAFi (dabrafenib) resulted in significantly
218 increased TSHR expression in ATC PDX models (**Fig. 4F-G**). While modest antitumor effects of
219 MEKi and/or BRAFi were observed, the main purpose of these experiments was to assess TSHR
220 upregulation upon MEKi and/or BRAFi treatment in PDX models of ATC. Collectively, these data
221 support the therapeutic strategy of MEKi and BRAFi treatment to re-express TSHR and thereby
222 reduce ATC resistance to TSHR-CART cell therapy.

223 **MAPK inhibition upregulates TSHR and sensitizes TSHR-CART cell therapy to**
224 **dedifferentiated thyroid cancer *in vitro***

225 We then tested if pretreatment with MEKi or MEKi/BRAFi enhanced TSHR-CART cell activity
226 against dedifferentiated thyroid cancer cell lines *in vitro.* The PDTC cell line, THJ-529, was
227 cocultured with trametinib alone or trametinib plus dabrafenib (10nM or 1μM for trametinib or
228 dabrafenib). After four days, THJ-529 cells were washed and assessed for TSHR expression by

229 flow cytometry. THJ-529 cells demonstrated modest but consistently increased TSHR expression
230 after treatment with MEKi or MEKi/BRAFi compared to vehicle-treated cells (**Fig. 5A**). THJ-529
231 cells were then washed to remove residual MAPK inhibitor and plated with TSHR-CART cells for
232 five additional days, at which point TSHR-CART cell proliferation was assessed via flow
233 cytometry. TSHR-CART cells demonstrated significantly more proliferation in response to THJ-
234 529 cells which were pretreated with trametinib or trametinib plus dabrafenib compared to vehicle
235 control-treated THJ-529 cells (**Fig. 5B**). Treatment with higher or more prolonged MAPK inhibitor
236 doses to further increase TSHR expression resulted in tumor cell death to the point where post-
237 coculture analyses could not be conducted; however, the modest TSHR upregulation observed
238 with low doses of MAPK inhibitors resulted in significantly increased TSHR-CART response. We
239 then assessed the sensitivity of TSHR-CART cells to low expression levels of TSHR. We
240 generated a series of TSHR$^+$ FTC-133 cells with varied levels of TSHR expression. TSHR$^+$ FTC-
241 133 cells had TSHR levels ranging from ~40,000 to 300,000 TSHR per cell, compared to ~6,000
242 TSHR per cell for our ATC PDX model, THJ560, and ~1,000 TSHR per cell for wildtype FTC-133
243 (**Fig. 5C-D**). TSHR-CART cells demonstrated potent cytotoxicity against all TSHR$^+$ FTC-133 cell
244 lines, with only the wildtype FTC-133 cells showing resistance to TSHR-CART cell killing (**Fig.
245 5E**). These findings indicated that low to moderate TSHR upregulation via MAPK inhibition leads
246 to robust antitumor activity of TSHR-CART cells.

247 **MAPK inhibition does not negatively impact TSHR-CART cell activity**

248 Therefore, we aimed to evaluate MEK and BRAF inhibition as a strategy to upregulate TSHR
249 expression on thyroid cancer cells and increase the therapeutic index of TSHR-CART cell
250 therapy. Given that T cells are shown to utilize MAPK signaling, we first tested for potential
251 detrimental effects of MEKi or MEKi/BRAFi on CART cell activity. TSHR-CART proliferation (**Fig.
252 6A**), killing (**Fig. 6B**), degranulation (**Supplemental Fig. S5A**), and intracellular cytokine
253 production (**Supplemental Fig. S5B**) were not affected by the addition of trametinib alone or
254 trametinib plus dabrafenib compared to media control. We next assessed the effects of prolonged

255 MAPK inhibition on TSHR-CART function through an exhaustion assay developed with repeated
256 CART activation.(*40*) Here, TSHR-CART cells were repeatedly stimulated with irradiated $TSHR^+$
257 FTC-133 cells along with vehicle control, 10nM trametinib, or 10nM trametinib plus 10nM
258 dabrafenib. After one week of chronic stimulation, TSHR-CART cells were isolated and cocultured
259 with fresh $TSHR^+$ FTC-133 cells and vehicle control, 10nM trametinib, or 10nM trametinib plus
260 dabrafenib for proliferation and cytotoxicity assays (**Supplemental Fig. S5C**). Here as well, the
261 addition of MAPK inhibitors did not appear to negatively impact TSHR-CART cell proliferation
262 (**Fig. 6C, Supplemental Fig. S5D**) or killing (**Fig. 6D**).

263 **Combination of TSHR-CART cells plus MAPK inhibitors yields superior TSHR-CART cell**
264 **activity**

265 Having shown that the addition of MAPK inhibitors was not detrimental to CART function, we next
266 studied the kinetics of TSHR expression after MEKi or MEKi/BRAFi to determine the longevity of
267 TSHR re-expression after treatment with MAPK inhibitors. Mice were implanted with $5mm^3$ Th-
268 560 ATC PDX tumors. When tumors reached ~$100mm^3$, mice were treated daily with either
269 vehicle control or with 1.5 mg/kg dual MEKi/BRAFi (R05126766) plus 1 mg/kg BRAFi
270 (dabrafenib). TSHR expression was assessed by IHC and was found to be significantly elevated
271 after 7 days of MAPK inhibitor treatment compared to vehicle control. However, TSHR expression
272 was subsequently lost within two days after stopping MAPK inhibitor treatment (**Supplemental**
273 **Fig. S6A-B**).

274 Given these results, we compared different dosing regimens of MEKi/BRAFi in combination with
275 TSHR-CART cell therapy in ATC PDX models to determine if sequential or concurrent MAPK
276 inhibitor administration yielded superior CART antitumor activity. Mice were subcutaneously
277 implanted with $5mm^3$ Th-560 ATC PDX tumors. When tumors reached ~$100mm^3$, mice
278 were randomized to daily treatment with vehicle control, 0.25 mg/kg trametinib (concurrently
279 administered until experimental endpoints or stopped after 7 days), or 0.25 mg/kg trametinib plus

280 2 mg/kg dabrafenib (concurrently administered until experimental endpoints or stopped after 7
281 days). Mice treated with vehicle control were engrafted with tumor one week later than mice
282 treated with MAPK inhibitors to ensure equal tumor sizes across all groups when UTD or TSHR-
283 CART cells were administered. As a further dose escalation, mice were then given 2 x 10^7 UTD
284 or TSHR-CART cells via tail vein injection. Tumor volume, body weight, and body condition were
285 inspected to monitor disease progression and to assess for endpoint criteria (**Fig. 7A**). Mice
286 treated with concurrent MEKi or concurrent MEKi plus BRAFi in combination with TSHR-CART
287 cells (CART + MEKi and CART + MEKi/BRAFi, respectively) showed superior antitumor efficacy
288 (**Fig. 7B-C, Supplementary Fig. S7A-F, Supplementary Fig. S8A-F**). We then performed a
289 followup experiment using 1 x 10^7 UTD or TSHR-CART cells. Here, mice with concurrent MAPK
290 inhibitor administration plus TSHR-CART cells demonstrated durable antitumor control lasting
291 beyond two months (**Supplementary Fig. S8G**). Given these results, we used the 1 x 10^7 TSHR-
292 CART dose in subsequent experiments. These findings indicate that administering MAPK
293 inhibitors concurrently with TSHR-CART cells enhances the antitumor activity of TSHR-CART
294 cell therapy.
295 We next assessed how long MAPK inhibitors needed to be administered concurrently with TSHR-
296 CART cell therapy for enhanced antitumor efficacy. Here, mice treated with UTD or TSHR-CART
297 cells were given vehicle control, MEKi/BRAFi for two weeks after CART administration,
298 MEKi/BRAFi, for four weeks after CART administration, or continuous MEKi/BRAFi after CART
299 administration until experimental endpoints were reached (**Fig. 7D**). Mice receiving the combination
300 of TSHR-CART and MAPK inhibitors showed superior tumor control and survival, regardless of the
301 duration of concurrent MAPK inhibitors (**Fig. 7E-F, Supplementary Fig. S9A-F**). This indicates that
302 using MAPK inhibitors in combination with TSHR CART cells for 2 weeks is sufficient to induce
303 TSHR upregulation and potent TSHR activity. Peripheral blood analysis at day 14 post-CART
304 injection showed comparable human T cell expansion in mice treated with TSHR-CART cells plus

305 vehicle control compared to mice treated with TSHR-CART cells plus MAPK inhibitors (**Fig. 7G**).

306 **DISCUSSION**

307 Here, we describe the development and evaluation of a highly translational CART cell therapy for
308 the treatment of poorly differentiated, anaplastic, and metastatic thyroid cancers. TSHR is a
309 rational target for CART cell therapy, given that it is widely expressed in thyroid cancers and rarely
310 expressed outside the thyroid. We subsequently generated and tested TSHR-CART cells, which
311 demonstrated antigen-specific activity against TSHR-expressing target cells *in vitro* and *in vivo*.
312 HCC represents ~4% of thyroid cancers and is typically radioiodine-resistant for metastatic
313 disease, retains TSHR expression, and currently has no FDA-approved therapy.(*7*) Our data
314 demonstrate that TSHR-CART cell therapy resulted in durable remissions *in vivo* and may
315 represent a treatment option for this subset of patients.

316 De-differentiated and anaplastic thyroid cancers can exhibit significant downregulation of thyroid
317 developmental genes, including TSHR.(*41, 42*) This phenomenon poses a formidable hurdle to
318 effective TSHR-CART treatment. Increasing evidence indicates that TSHR downregulation and
319 de-differentiation is mediated by MAPK signaling.(*28, 29, 34, 43, 44*) The majority of thyroid
320 cancers have activating oncogenic gene mutations involving PI3K, RET, RAS, and BRAF.(*32*)
321 Constitutive activation of these proteins stimulates MAPK signaling, inhibiting the expression of
322 thyroid hormone biosynthesis genes.(*33, 34*) Therefore, when BRAF activation is switched off
323 genetically or its downstream signaling is inhibited with MEKi or BRAFi, tumors re-express TSHR
324 and reaccumulate iodine. Such a strategy has been employed in the clinic to enhance the
325 response to radioactive iodine therapy.(*30*) Recent findings from patients with thyroid cancer who
326 have been treated with MEKi indicate a dramatic upregulation of TSHR within both primary and
327 secondary thyroid cancer tumors.(*30, 45*) Additionally, MEKi, alone or in combination with
328 BRAFi, demonstrate significant antitumor activity in metastatic thyroid cancer and are FDA-
329 approved for ATC.(*46*) We therefore tested the combination of TSHR-CART cell therapy plus
330 MAPK inhibition to upregulate TSHR expression in the tumor and enhance CART efficacy,

331 demonstrating restoration of TSHR expression and improved CART antitumor effects in mice
332 receiving combination therapy compared to mice receiving CART monotherapy.
333 Major limitations to effective CART cell therapy in solid tumor settings include appropriate target
334 antigen selection, antigen-negative escape, and lack of T cell infiltration into the tumor site. The
335 treatment strategy we have outlined here has strong potential to overcome these limitations, as
336 TSHR is nearly uniquely and universally expressed in thyroid tumors, MAPK inhibition induces
337 TSHR re-expression, and TSHR-expressing advanced thyroid tumors are commonly infiltrated by
338 immune cells, including T cells.(*9*)
339 Regarding the potential for on-target off-tumor toxicity, consistent with publicly available datasets,
340 our tissue microarray demonstrates that TSHR expression is mainly limited to the thyroid gland.
341 Furthermore, our CAR is cross reactive with mouse TSHR and we did not observe any toxicities
342 in our mouse experiments. As patients with aggressive thyroid cancers will have undergone
343 previous thyroidectomy, there will be no healthy thyroid tissue remaining upon treatment with
344 TSHR-CART cells. There have also been reports of extra-thyroidal TSHR expression and
345 function. Aberrant TSHR expression has been documented in the orbital fibroblasts of patients
346 with Graves' disease in the context of thyroid associated ophthalmopathy, and TSHR-targeted
347 treatments have shown clinical responses.(*47-51*) However, thyroid cancers have not been
348 associated with thyroid associated ophthalmopathy. As such, it is not probable that orbital/ocular
349 toxicities will arise with TSHR CART cell therapy. We also have not oberved any orbital toxicity in
350 our mouse models. In addition, K1-70, the TSHR antibody from which we derived the scFv for our
351 TSHR-CAR, was found to be well-tolerated at all dose levels in a phase I trial for patients with
352 Graves' disease, (*52*) and in a patient with both follicular thyroid cancer and Graves' disease.(*53*)
353 These clinical studies, while still nascent, demonstrate a promising safety profile. Vigilant
354 monitoring for orbital toxicities will be incorporated into our phase I clinical trial.
355 CART cells targeted against ICAM-1(*54*) and GFRα4(*55*) have demonstrated efficacy in preclinical
356 thyroid cancer models. Recently, TSHR-CART cell therapy displayed potent activity against

357 human thyroid cancer models *in vivo.*(*38*) Furthermore, two patients with high metastatic burden
358 and iodine-131-resistant thyroid cancer demonstrated a complete response (CR) and a near CR
359 three months after TSHR-CART treatment. The first patient, who had papillary thyroid carcinoma,
360 sustained CR until one year post-TSHR-CART infusion, indicating potential for long-term
361 antitumor responses.(*56*) However, these studies focused on differentiated thyroid cancers with
362 high TSHR expression. One patient with iodine-refractory, metastatic PDTC was treated with
363 CART cells targeting both TSHR and CD19. This patient achieved stable disease at day 30 post-
364 CART infusion and partial response 90 days post-CART infusion. While IHC demonstrated strong
365 TSHR expression pre-CART infusion, it is unknown if TSHR was downregulated after the start of
366 TSHR-CART cell therapy, leading to underwhelming therapeutic response in this dedifferentiated
367 thyroid cancer setting.(*57*)
368 Several reports have shown conflicting results regarding the potential impacts of MAPK inhibitors
369 on T cell function. One study found that dabrafenib did not suppress human T cell function, but
370 trametinib led to an incomplete and transient inhibition of T cell proliferation and cytokine
371 production. The addition of dabrafenib to trametinib was found to offset the negative effects of
372 trametinib on T cell function *in vitro.* Further, trametinib did not appear to have detrimental effects
373 on T cells, but rather increased tumor infiltration of T cells *in vivo*.(*58*) Another study found that
374 BRAFi also enhanced tumor infiltration of adoptively transferred T cells in mice.(*59*) Other reports
375 showed that MEKi led to reprogramming of CD8 T cells to stem cell memory phenotypes and
376 thereby enhanced antitumor activity.(*60*) Another group reported that MEKi during chronic T cell
377 stimulation ameliorated terminal T cell exhaustion by slowing the transcription rates of effector-
378 and terminal- exhaustion-related genes, reducing nutrient uptake and mitochondrial ROS
379 accumulation, and ultimately enhancing the persistence of tumor-infiltrating lymphocytes *in*
380 *vivo*.(*61*) An early report of the impacts on MAPK inhibitors on CART cells showed that trametinib
381 plus dabrafenib across a range of concentrations inhibited GD2-targeted patient-derived CART
382 cell activation, cytokine production, and cytotoxicity; however, the authors suggested that strong

383 stimulation of the CAR with GD2^{high} tumor cells had the potential to overcome the detrimental
384 effects of MAPK inhibitors on CART functions.(*62*) Another GD2-CART study confirmed that
385 trametinib inhibited CART cytotoxic abilities and cytokine secretion *in vitro*, but *in vivo*, trametinib
386 in combination with GD2-CART resulted in enhanced tumor suppression compared to
387 monotherapy treatment groups.(*63*) Another group showed that, while the combination of
388 trametinib and dabrafenib did negatively impact CSPG4-targeted CART cell *in vitro* functions,
389 these effects were milder than those seen with other MAPK inhibitor combinations.(*64*) Recently,
390 it was reported that MEKi reduced CART cell activation, exhaustion, apoptosis, and terminal
391 differentiation across multiple different CAR constructs in both solid and liquid tumors through
392 downregulation of c-Fos and JunB.(*65*) While consensus has yet to be reached, more recent
393 studies demonstrate that potential negative impacts of MAPK inhibitors on T cell function are
394 nuanced and context-dependent, and MAPK inhibitors may actually enhance CART function in a
395 variety of settings.
396 We present TSHR-CART cell therapy in combination with MAPK inhibition as a sensitizing
397 modality, representing a major step forward in the development of a treatment strategy for PDTC
398 and ATC as well as DTCs which have become refractory to radioiodine therapy. Based on these
399 data, we are planning to launch a phase I clinical trial for TSHR-CART cell therapy as a
400 monotherapy in patients with TSHR^{high} metastatic thyroid cancers and in combination with MAPK
401 inhibitors in patients with TSHR^{low} metastatic thyroid cancers.
402

403 **MATERIALS AND METHODS**

404 **Study design**

405 This study aimed to assess the efficacy of TSHR-CART cell therapy as a monotherapy in TSHR^{high}
406 thyroid cancers and in combination with MAPK inhibitors in TSHR^{low} thyroid cancers. First, the
407 expression of TSHR was assessed and verified on patient clinical samples utilizing IHC and tissue
408 microarray tools. Second, we designed and engineered human CART cells targeting TSHR

409 (TSHR-CART), that were subjected to various *in vitro* and vivo *assays* to assess their effector
410 functions (cytotoxicity, proliferation, degranulation and cytokine production). Third, we tested the
411 addition of MAPK inhibitors *in vitro* to assess their upregulation of TSHR and sensitization prior
412 to TSHR-CART treatment. Lastly, we performed *in vivo* assays to assess CART cell antitumor
413 activity in combination with MAPK inhibitors in a concurrent or sequential fashion. For each
414 experiment, the number of independent experiments (*n*) is specified in the figure legends. For *in*
415 *vivo* assays, NGS mice were utilized, and they were randomly assigned to control and
416 experimental groups, and the study was not blinded. Data collection was stopped at the
417 predetermined times. Human endpoint criteria were determined when mice presented above 20%
418 lost weight and tumor exceeded 700 mm^3. No data was excluded from analysis. Sample sizes
419 are indicated in the figure legends.

420 **Reagents**

421 Detailed information on all reagents used in this article is listed in Supplementary Table S1.

422 **Cell lines**

423 FTC-133, XTC.UC1, and THJ-529T cell lines were graciously provided by Dr. Copland's lab in
424 Mayo Clinic, Jacksonville, Florida. The FTC-133 cell line is derived from a differentiated follicular
425 thyroid carcinoma with known mutations that include *FLCN, MSH6, NF1, PTEN, TERT*, and *TP53*
426 (https://www.cellosaurus.org/CVCL_1219). The THJ-529T cell line was derived from a PDTC
427 tumor containing *BRAF* and *TERT* mutations (https://www.cellosaurus.org/CVCL_9916).(*66*)
428 XTC.UC1 is the only characterized HCC cell line and the only known cell line to continue to
429 express endogenous TSHR *in vitro*.(*67*) All cell lines were DNA short tandem repeat (STR)
430 validated prior to use. For indicated experiments, THJ-529 and FTC-133 cell lines were
431 transduced with a firefly luciferase (Luc^+) vector containing a hygromycin resistance gene
432 (Promega, Madison, WI, USA) as well as a TSHR vector and a puromycin resistance gene
433 (Genecopoeia Inc., Rockville, MD, USA). These cells were then cultured in selection media
434 containing either hygromycin (1 µg/mL) or puromycin (1 µg/mL) to obtain a pure population as

435 previously described.(*68*) FTC-133 and XTC.UC1 cell lines were cultured in D10 medium made
436 with DMEM (Corning Inc., Corning, NY, USA), 10% FBS (Sigma, St. Louis, MO, USA), and 1%
437 PSG (Gibco, Gaithersburg, MD, USA). For specific *in vitro* assays, FTC-133 cell lines were
438 transduced with different MOIs of a TSHR vector containing puromycin resistance gene
439 (Genecopoeia Inc., Rockville, MD, USA), and TSHR absolute counts were determined by flow
440 cytometry using absolute counting beads (CountBright™, Invitrogen, Carlsbad, CA, USA).
441 Mycoplasma testing was performed and confirmed to be negative monthly.

442 **CAR construct and CART cell production**

443 The use of recombinant DNA in the laboratory was approved by the Mayo Clinic Institutional
444 Biosafety Committee (IBC), IBC number HIP00000252.20. Peripheral blood mononuclear cells
445 (PBMCs) were isolated from de-identified normal donor blood apheresis cones(*69*) obtained
446 under a Mayo Clinic IRB approved protocol, using SepMate tubes (STEMCELL Technologies,
447 Vancouver, BC, Canada) and Lymphoprep™ solution (STEMCELL Technologies, Vancouver,
448 BC, Canada). T cells were separated with negative selection magnetic beads using EasySep™
449 Human T Cell Isolation Kit (STEMCELL Technologies, Vancouver, BC, Canada). Second-
450 generation 4-1BB- costimulated TSHR CAR constructs were synthesized *de novo* (IDT, Coralville,
451 USA) and cloned into a third-generation lentivirus under the control of the EF-1α promotor. The
452 TSHR-targeted single chain variable fragment was derived from an autoantibody from a patient
453 with Graves' disease, clone K1-70.(*70*) TSHR-CART cells were then generated through the
454 lentiviral transduction of normal donor T cells as previously described(*71, 72*). Briefly, lentiviral
455 particles were generated through the transient transfection of plasmid into 293T virus-producing
456 cells (ATCC, Manassas, VA, USA) in the presence of Lipofectamine 3000 (Invitrogen, Carlsbad,
457 CA, USA), vesicular stomatitis virus G (VSV-G), and packaging plasmids pCMVR8.74 (Addgene,
458 Cambridge, MA, USA). The titers and multiplicity of infection (MOI) were analyzed and calculated
459 by flow cytometry as previously described.(*68*) T cells isolated from normal donors were stimulated

460 using anti-CD3/CD28 Dynabeads (Life Technologies, Oslo, Norway) at a 3:1 beads-to-cell ratio
461 and then transduced 24 hours after stimulation with lentivirus particles at a MOI of 3. T cells were
462 cultured in T cell medium containing X-VIVO™ 15 media (Lonza, Basel, Switzerland), 10% human
463 AB serum (Corning Inc., Corning, NY, USA), and 1% PSG (Gibco, Gaithersburg, MD, USA).
464 Magnetic bead removal and the evaluation of CAR expression on T cells by flow cytometry were
465 performed on day 6 by staining with a goat anti-human IgG H+L secondary antibody (Invitrogen,
466 Carlsbad, CA, USA). CART cells were harvested and cryopreserved on day 8 for future
467 experiments. Prior to cryopreservation, CART cells were stained and evaluated to assess T-cell
468 subset and phenotype expression patterns using the following antibodies: CD45 APC (BioLegend,
469 San Diego, CA, USA), CD3 BV605 (BioLegend), CD4 PE-Cy7 (BD Biosciences, Franklin Lakes, NJ,
470 USA), CD8 BV421 (BD Biosciences), CCR7 PE (BioLegend) and CD45RA APC-Cy7 (BioLegend).
471 CART cells were thawed and rested in T cell medium overnight at 37°C and 5% CO_2 prior to
472 experimental use.

473 **Multi-parametric flow cytometry**

474 Samples were prepared for flow cytometry as previously described.(*68, 71-74*) In all analyses,
475 the population of interest was gated based on forward vs side scatter characteristics, then by
476 singlet gating, and then by live cell gating using LIVE/DEAD™ Fixable Aqua Dead Cell Stain Kit
477 (Invitrogen, Carlsbad, CA, USA). Flow cytometry was performed on a three-laser CytoFLEX
478 (Beckman Coulter, Chaska, MN, USA). All analyses were performed using FlowJo v10.7.1
479 software (Ashland, OR, USA).

480 **Immunohistochemistry (IHC)**

481 IHC was performed on paraffin-embedded tissue. Thyroid tissue microarray (TMA) was made
482 from archival samples under Mayo Clinic IRB approval with sample size for each tumor at 1.5 mm.
483 Paraffin blocks were cut into 5 μm thick sections. Slides were deparaffinized, rehydrated with
484 decreasing concentrations of ethanol, and finally with water. Additionally, a normal human tissue
485 microarray was purchased (Bio SB, Santa Barbara, CA, USA), which included 23 different normal

486 human tissue types. Antigen retrieval was performed using Antigen Retrieval Solution (pH 6 or pH
487 9) (Dako, Glostrup, Denmark) for at least 15 minutes in an autoclave, and cooling for 30 minutes
488 at room temperature. Slides were washed with 3% hydrogen peroxide (Fisher Scientific, Waltham,
489 MA, USA) for 10 minutes to block the activity of endogenous peroxidases. Primary anti-human
490 TSHR antibody was used for 60 minutes at room temperature at 1:500 (abcam, ab218108,
491 Cambridge, UK). The infiltration of human T lymphocytes into tumors was assessed using anti-
492 human CD3 at 1:500 (abcam, ab52959, Cambridge, UK). The primary antibody was detected
493 using the Envision Labeled Kit (Dako, Glostrup, Denmark) according to the manufacturer's
494 protocol. After washing, slides were counterstained with Mayer's hematoxylin (Sigma-Aldrich, St.
495 Louis, MO, USA). Slides were dehydrated through ethanol and xylene and cover-slipped using a
496 xylene-based mounting medium (Fisher Scientific). Samples were examined under bright-field
497 illumination at 20x objective, and digital images were obtained using Aperio AT2 (Leica, Wetzlar,
498 Germany). Results were processed using Aperio eSlide Manager and H-Score values were
499 estimated using the Aperio ImageScope Software (both Aperio Technologies, Vista, CA, USA).
500 The staining of the TMA punches was scored using an algorithm in the Imagescope Software
501 (Aperio Technologies) created by a histologist based upon signal intensity (0, 1C, 2C, 3C). H
502 score was then calculated based upon signal intensity and percentage:
503 HZ(1C%!1)(2C%!2)(3C%!3). Cases were excluded from the study if a section could not be
504 assigned a score due to insufficient quantity of tumor tissue present**.** Normal tissues were used
505 as a positive and negative control.
506 For cell line preparation for IHC, cells were washed three times with PBS (Corning, NY, USA),
507 scraped from the bottom of the plate using a cell lifter (Fisherbrand, Waltham, MA, USA),
508 transferred to 50 mL polypropylene tubes and centrifuged at room temperature for 2 minutes at
509 500 x g. The supernatant was aspirated, and 10% neutral buffered formalin (Fisher Scientific)
510 was added for 30 minutes at room temperature. HistoGel (Thermo Scientific) was heated in the
511 microwave for 3 seconds at maximal power and converted to a liquid state. Cells were transferred

512 to the HistoScreen Tissue Cassettes (Thermo Scientific) and covered with liquid Histogel.
513 Samples were placed at room temperature and allowed to solidify. HistoGel blocks were
514 transferred into tissue embedding cassettes (Thomas Scientific, Swedesboro, NJ, USA),
515 dehydrated in increasing concentrations of ethanol, xylene, and paraffin embedding. Sections
516 were prepared as described in the immunohistochemistry section. Primary anti-human TSHR
517 antibody was used for 60 minutes at room temperature at 1:1500 (abcam, ab218108, Cambridge,
518 UK). Envision labeled polymer (Dako, Glostrup, Denmark) was used for 30 minutes as a
519 secondary antibody. Slides were stained with diaminobenzidine tetrahydrochloride (DAB)
520 chromogen (Dako) for 5 minutes at room temperature and counterstained with Mayer's
521 hematoxylin (Sigma-Aldrich, St. Louis, MO, USA). Control staining with hematoxylin and eosin
522 (Sigma-Aldrich) was also performed. Aperio AT2 scanner (Leica, Wetzlar, Germany) was used
523 for the digital image, at 20x objective. Images were analyzed using the Aperio ImageScope
524 software (Aperio Technologies).

525 **Immunocytochemistry (ICC)**

526 THJ-529 cells (2 x 10^4 cells/chamber) were plated in a 4-well chamber slide (Nunc, Thermo
527 Scientific, Waltham, MA, USA), incubated overnight. After 24 hours, media was aspirated, and
528 cells were washed three times with PBS (Corning, NY, USA). Then, 2% paraformaldehyde was
529 added for 20 minutes at room temperature. Again, cells were washed three times with PBS. Next,
530 ice-cold 100% methanol (Fisher Scientific) was added for 7 minutes at -20°C. Methanol was
531 aspirated, and samples were allowed to air dry for 10 minutes. Next, serum-free-blocking diluent
532 (Dako) was used for 30 minutes at room temperature. Primary anti-human TSHR antibody was
533 used for 60 minutes at room temperature at 1:1500 (abcam, ab218108, Cambridge, UK). Slides
534 were subsequently prepared as described in the immunohistochemistry section.

535 ***In vitro* T cell function assays**

536 Cytotoxicity assays were performed as previously described.(*68, 71-74*) Wildtype ($TSHR^-$) Luc^+

537 FTC-133, TSHR$^+$ Luc$^+$ FTC-133, wildtype (TSHR$^-$) Luc$^+$ THJ-529, or TSHR$^+$ Luc$^+$ THJ-529 cells
538 were used as target cells. UTD or TSHR-CART cells were co-cultured with target cells at various
539 effector: target (E:T) ratios in T cell medium. Cytotoxicity was calculated by bioluminescence
540 imaging on the Promega GloMax Explorer (Promega Corporation, Fitchburg, WI, USA) as a
541 measure of residual live cells at indicated time points. Samples were treated with 1µL D-luciferin
542 (30µg/mL) per 100µL sample volume (Gold Biotechnology, St. Louis, MO, USA) prior to imaging.
543 Proliferation assays were performed utilizing two approaches as previously described.(*68, 71-74*)
544 Briefly, for the first approach, TSHR-CART cells were stained with CFSE (Invitrogen) cell dye on
545 day 0, then washed and counted prior to being plated at a 1:1 E:T ratio with target cell lines. Each
546 assay included T cells with media only as a negative control and T cells with PMA and ionomycin
547 as a positive control. On day 5, percent of CFSE CART cells was determined via flow cytometry
548 after staining with APC-H7 anti-human CD3 (BD Biosciences) and Zombie R718™ (BioLegend)
549 dye. Alternatively, the same assay was repeated but without the addition of CFSE and with
550 LIVE/DEAD™ Fixable Aqua as the viability dye.
551 For *in vitro* experiments testing the cytotoxic and proliferation effects of TSHR-CART cells
552 exposed to different levels of TSHR on target cells, TSHR-CART cells were co-cultured with FTC-
553 133 tumor cells expressing different levels of TSHR and cytotoxicity and proliferation was
554 measured as described above.
555 For cytokine assays, media was collected on day 3 of co-culture of TSHR-CART cells with target
556 cells, and supernatants were isolated and purified via centrifugation as previously described(*71*).
557 Supernatants were prepared following manufacturer's protocol for the MILLIPLEX® Human
558 Cytokine/Chemokine/Growth Factor Panel A 38 Plex Premixed Magnetic Bead Panel (Millipore
559 Sigma, Ontario, Canada). Cytokine data was collected using a Luminex LX200 (Millipore Sigma).
560 For degranulation assays (*68, 71*), UTD or TSHR-CART cells were incubated with various target
561 cells at an E:T ratio of 1:5, and antibodies against CD107a FITC (BD Biosciences), CD28 (BD
562 Biosciences), and CD49d (BD Biosciences), as well as monensin (BioLegend), were added at the

563 start of the incubation. After 4 hours, cells were harvested and stained with LIVE/DEAD™ Fixable
564 Aqua. Cells were then fixed and permeabilized (FIX & PERM Cell Fixation & Cell Permeabilization
565 Kit, Life Technologies, Oslo, Norway) and stained for CD3 APC (, eBioscience, San Diego, CA,
566 USA) and intracellular cytokines including IL-2 PE CF594 (BD Horizon), GM-SCF BV421 (BD
567 Horizon) and MIP-1β Pe-Cy7 (BD Pharmigen).
568 For *in vitro* assays performed to assess the impact of MAPK inhibitors on TSHR-CART cells,
569 TSHR-CART cells were cultured with target tumor cells or media alone, along with either vehicle
570 control (DMSO), trametinib (10nM) alone, or trametinib plus dabrafenib (10nM). Effector functions
571 of TSHR-CART cells (proliferation, cytotoxicity, degranulation and cytokine profile) were
572 assessed as described above. Alternatively, TSHR-CART cells were cocultured in an *in vitro*
573 model for CART cell exhaustion previously described by our laboratory.(*40*) Here, TSHR-CART
574 cells were cultured at a 1:1 ratio with irradiated target cells along with either vehicle control
575 (DMSO), trametinib (10nM) alone, or trametinib plus dabrafenib (10nM). Drug-containing media
576 and irradiated target cells were added to the TSHR-CART cell cocultures every other day for 7
577 days. Then, chronically stimulated TSHR-CART cells were isolated using CD4 (Miltenyi Biotec,
578 Auburn, CA, USA) and CD8 (Miltenyi Biotec) microbeads and were subsequently plated with
579 fresh, non-irradiated target cells to assess cytotoxic and proliferative capacities as described
580 above.
581 ***In Vivo* Models**
582 Male and female 6-8-week-old NSG mice were purchased (Jackson Laboratories, Bar Harbor,
583 ME, USA) and maintained in an animal barrier space that is approved by the institutional Biosafety
584 Committee for BSL2+ level experiments at the Mayo Clinic animal facility (IBC
585 #HIP00000252.20). Mice were treated on an IACUC-approved protocol (A00001767).
586 **XCT.UC1 model:** The purpose of this model was to test initial TSHR-CART activity in a thyroid
587 cancer model which retains endogenous TSHR expression *in vivo*. XCT.UC1 is a Hurtle cell
588 carcinoma cell line which retains TSHR expression when passaged in mice but not *in vitro*. 1 x

589 10^7 XTC.UC1 cells were suspended in a 50% Matrigel basement medium and subcutaneously
590 injected into the rear flank of NSG mice. Serial caliper measurements were performed to confirm
591 tumor engraftment. Mice were then randomized based on tumor burden to receive 1 x 10^7 UTD
592 or TSHR-CART. Tumor growth was monitored by serial caliper measurements (width x height x
593 length x 0.523 = mm^3). Mice were euthanized once IACUC-approved endpoint criteria were met,
594 and remaining tumors were collected for IHC as indicated in each specific experiment.
595 **TSHR$^+$ THJ-529 model:** The purpose of this model was to assess a TSHR-CART dose
596 escalation. TSHR$^+$ THJ-529 is a poorly differentiated thyroid cancer cell line made to overexpress
597 TSHR. 2.5 x 10^6 TSHR$^+$ THJ-529 cells were suspended in a 50% Matrigel basement medium and
598 subcutaneously injected into the rear flank of NSG mice. Serial caliper measurements were
599 performed to confirm tumor engraftment. Mice were then randomized based on tumor burden to
600 receive 5 x 10^6 UTD, 5 x 10^6 TSHR-CART, or 1 x 10^7 TSHR-CART. Tumor growth was monitored
601 by serial caliper measurements (width x height x length x 0.523 = mm^3). Mice were euthanized
602 once IACUC-approved endpoint criteria were met, and remaining tumors were collected for IHC
603 as indicated in each specific experiment.
604 **TH-560 model:** The purpose of this model was to assess TSHR upregulation or TSHR-CART
605 activity after MAPKi administration. This model reflects the strategy of TSHR-CART and MAPK
606 inhibitor combination to be used in patients with ATC. TH-560 is an ATC PDX with downregulated
607 TSHR expression. All NSG mice were surgically engrafted with $5mm^3$ ATC PDX TH-560 tumors
608 in the rear flank. In TSHR upregulation experiments, mice were treated with the indicated doses of
609 MEKi/BRAFi (trametinib, dabrafenib, or R05126766). Upon euthanasia, tumors were harvested for
610 IHC.
611 In the MAPK inhibitor and TSHR-CART combination experiments, upon tumor engraftment, mice were
612 treated with a sub-therapeutic dose of 1mg/kg trametinib and 1.5mg/kg dabrafenib as a sensitizing
613 regimen to induce TSHR expression on ATC tumor cells. On Day 7, additional mice were surgically

614 engrafted with 5mm^3 ATC PDX tumors in the same manner as the first arm but were treated with
615 placebo rather than MAPK inhibitors. In the first MAPK inhibitor and TSHR-CART combination
616 experiment, in which mice were treated sequentially or concurrently with MEKi/BRAFi and TSHR-
617 CART cells, all mice were randomized based on tumor burden when tumors reached ~100mm^3
618 and injected with 2 x 10^7 UTD or TSHR-CART; this higher TSHR-CART dose was a further dose
619 escalation experiment. In the second MAPK inhibitor and TSHR-CART combination experiment, in
620 which mice were treated concurrently with MEKi/BRAFi and TSHR-CART cells with various
621 MEKi/BRAFi treatment stopping points, all mice were randomized based on tumor burden when
622 tumors reached ~100mm^3 and injected with 1 x 10^7 UTD or TSHR-CART. This lower dose of
623 TSHR-CART was used since no further treatment benefit was observed with the higher 2 x 10^7
624 dose. For all mice in the MAPK inhibitor and TSHR-CART combination experiments, tumor growth
625 was monitored by serial caliper measurements (width x height x length x 0.523 = mm^3). Weekly
626 tail vein bleeding after injection of CART cells was performed to assess T cell expansion. Mouse
627 peripheral blood was lysed using BD FACS Lyse (BD Biosciences) and then analyzed with flow
628 cytometry as previously described.(*68*) Mice were euthanized at IACUC-approved endpoints.

629 **Statistical analysis**

630 GraphPad Prism (La Jolla, CA, USA) and Microsoft Excel (Microsoft, Redmond, WA, USA) were
631 used to analyze raw experimental data. Statistical tests are described in figure legends.

632 **Author Contributions:** CMR, ELS, and JJG wrote, reviewed, and edited the manuscript,
633 designed and performed experiments, and analyzed data. JJG, JLM, EEM, AAD, TNH, GED,
634 LKM, BLK, EET, RLS, ELS, MLP, AAD, CMS, IC, OLS, KY, JMF, OLGR, HX, MHT, KJS, and
635 EJO aided in data collection. GO aided in patent and intellectual property management. YQ, HWT,
636 RCS, and AZ aided in data collection and troubleshooting. JAC and SSK formulated the initial
637 concept, designed experiments, supervised the study, and wrote the manuscript. All authors
638 edited and approved the final version of the manuscript.

639 **REFERENCES**

640 1. C. M. Kitahara, J. A. Sosa, Understanding the ever-changing incidence of thyroid cancer.
641 *Nat Rev Endocrinol* **16**, 617-618 (2020).
642 2. J. Kim, J. E. Gosnell, S. A. Roman, Geographic influences in the global rise of thyroid
643 cancer. *Nat Rev Endocrinol* **16**, 17-29 (2020).
644 3. H. Lim, S. S. Devesa, J. A. Sosa, D. Check, C. M. Kitahara, Trends in Thyroid Cancer
645 Incidence and Mortality in the United States, 1974-2013. *JAMA* **317**, 1338-1348 (2017).
646 4. R. C. Smallridge, J. A. Copland, Anaplastic thyroid carcinoma: pathogenesis and
647 emerging therapies. *Clin Oncol (R Coll Radiol)* **22**, 486-497 (2010).
648 5. C. K. Jung, A. Bychkov, K. Kakudo, Update from the 2022 World Health Organization
649 Classification of Thyroid Tumors: A Standardized Diagnostic Approach. *Endocrinol Metab*
650 *(Seoul)* **37**, 703-718 (2022).
651 6. S. Ahmadi, M. Stang, X. S. Jiang, J. A. Sosa, Hurthle cell carcinoma: current perspectives.
652 *Onco Targets Ther* **9**, 6873-6884 (2016).
653 7. D. G. McFadden, P. M. Sadow, Genetics, Diagnosis, and Management of Hurthle Cell
654 Thyroid Neoplasms. *Front Endocrinol (Lausanne)* **12**, 696386 (2021).
655 8. D. Viola, L. Valerio, E. Molinaro, L. Agate, V. Bottici, A. Biagini, L. Lorusso, V. Cappagli,
656 L. Pieruzzi, C. Giani, E. Sabini, P. Passannati, L. Puleo, A. Matrone, B. Pontillo-Contillo,
657 V. Battaglia, S. Mazzeo, P. Vitti, R. Elisei, Treatment of advanced thyroid cancer with
658 targeted therapies: ten years of experience. *Endocr Relat Cancer* **23**, R185-205 (2016).
659 9. J. D. French, Immunotherapy for advanced thyroid cancers - rationale, current advances
660 and future strategies. *Nat Rev Endocrinol* **16**, 629-641 (2020).
661 10. A. Maniakas, R. Dadu, N. L. Busaidy, J. R. Wang, R. Ferrarotto, C. Lu, M. D. Williams, G.
662 B. Gunn, M. C. Hofmann, G. Cote, J. Sperling, N. D. Gross, E. M. Sturgis, R. P. Goepfert,
663 S. Y. Lai, M. E. Cabanillas, M. Zafereo, Evaluation of Overall Survival in Patients With
664 Anaplastic Thyroid Carcinoma, 2000-2019. *JAMA Oncol* **6**, 1397-1404 (2020).

665 11. C. H. June, M. Sadelain, Chimeric Antigen Receptor Therapy. **379**, 64-73 (2018).
666 12. S. J. Schuster, M. R. Bishop, C. S. Tam, E. K. Waller, P. Borchmann, J. P. McGuirk, U.
667 Jäger, S. Jaglowski, C. Andreadis, J. R. Westin, I. Fleury, V. Bachanova, S. R. Foley, P.
668 J. Ho, S. Mielke, J. M. Magenau, H. Holte, S. Pantano, L. B. Pacaud, R. Awasthi, J. Chu,
669 Ö. Anak, G. Salles, R. T. Maziarz, Tisagenlecleucel in Adult Relapsed or Refractory
670 Diffuse Large B-Cell Lymphoma. **380**, 45-56 (2018).
671 13. S. S. Neelapu, F. L. Locke, N. L. Bartlett, L. J. Lekakis, D. B. Miklos, C. A. Jacobson, I.
672 Braunschweig, O. O. Oluwole, T. Siddiqi, Y. Lin, J. M. Timmerman, P. J. Stiff, J. W.
673 Friedberg, I. W. Flinn, A. Goy, B. T. Hill, M. R. Smith, A. Deol, U. Farooq, P. McSweeney,
674 J. Munoz, I. Avivi, J. E. Castro, J. R. Westin, J. C. Chavez, A. Ghobadi, K. V. Komanduri,
675 R. Levy, E. D. Jacobsen, T. E. Witzig, P. Reagan, A. Bot, J. Rossi, L. Navale, Y. Jiang, J.
676 Aycock, M. Elias, D. Chang, J. Wiezorek, W. Y. Go, Axicabtagene Ciloleucel CAR T-Cell
677 Therapy in Refractory Large B-Cell Lymphoma. *N Engl J Med* **377**, 2531-2544 (2017).
678 14. N. C. Munshi, L. D. Anderson, Jr., N. Shah, D. Madduri, J. Berdeja, S. Lonial, N. Raje, Y.
679 Lin, D. Siegel, A. Oriol, P. Moreau, I. Yakoub-Agha, M. Delforge, M. Cavo, H. Einsele, H.
680 Goldschmidt, K. Weisel, A. Rambaldi, D. Reece, F. Petrocca, M. Massaro, J. N. Connarn,
681 S. Kaiser, P. Patel, L. Huang, T. B. Campbell, K. Hege, J. San-Miguel, Idecabtagene
682 Vicleucel in Relapsed and Refractory Multiple Myeloma. *N Engl J Med* **384**, 705-716
683 (2021).
684 15. S. L. Maude, T. W. Laetsch, J. Buechner, S. Rives, M. Boyer, H. Bittencourt, P. Bader, M.
685 R. Verneris, H. E. Stefanski, G. D. Myers, M. Qayed, B. De Moerloose, H. Hiramatsu, K.
686 Schlis, K. L. Davis, P. L. Martin, E. R. Nemecek, G. A. Yanik, C. Peters, A. Baruchel, N.
687 Boissel, F. Mechinaud, A. Balduzzi, J. Krueger, C. H. June, B. L. Levine, P. Wood, T.
688 Taran, M. Leung, K. T. Mueller, Y. Zhang, K. Sen, D. Lebwohl, M. A. Pulsipher, S. A.
689 Grupp, Tisagenlecleucel in Children and Young Adults with B-Cell Lymphoblastic
690 Leukemia. *N Engl J Med* **378**, 439-448 (2018).

691 16. G. L. Beatty, E. K. Moon, Chimeric antigen receptor T cells are vulnerable to
692 immunosuppressive mechanisms present within the tumor microenvironment.
693 *Oncoimmunology* **3**, e970027 (2014).
694 17. M. Castellarin, K. Watanabe, C. H. June, C. C. Kloss, A. D. Posey, Driving cars to the
695 clinic for solid tumors. *Gene Therapy* **25**, 165-175 (2018).
696 18. S. Ma, X. Li, X. Wang, L. Cheng, Z. Li, C. Zhang, Z. Ye, Q. Qian, Current Progress in
697 CAR-T Cell Therapy for Solid Tumors. *Int J Biol Sci* **15**, 2548-2560 (2019).
698 19. B. Moghimi, D. Barrett, CAR T Cells for Solid Tumors. *Current Stem Cell Reports* **3**, 269-
699 278 (2017).
700 20. R. C. Sterner, R. M. Sterner, CAR-T cell therapy: current limitations and potential
701 strategies. **11**, 69 (2021).
702 21. L. A. Kankeu Fonkoua, O. Sirpilla, R. Sakemura, E. L. Siegler, S. S. Kenderian, CAR T
703 cell therapy and the tumor microenvironment: Current challenges and opportunities. *Mol*
704 *Ther Oncolytics* **25**, 69-77 (2022).
705 22. I. Can, M. J. Cox, E. L. Siegler, R. Sakemura, S. S. Kenderian, Challenges of chimeric
706 antigen receptor T-cell therapy in chronic lymphocytic leukemia: lessons learned. *Exp*
707 *Hematol* **108**, 1-7 (2022).
708 23. R. Sakemura, M. Hefazi, E. L. Siegler, M. J. Cox, D. P. Larson, M. J. Hansen, C.
709 Manriquez Roman, K. J. Schick, I. Can, E. E. Tapper, P. Horvei, M. M. Adada, E. D.
710 Bezerra, L. A. Kankeu Fonkoua, M. W. Ruff, W. Nevala, D. K. Walters, S. A. Parikh, Y.
711 Lin, D. F. Jelinek, N. E. Kay, P. L. Bergsagel, S. S. Kenderian, Targeting Cancer-
712 Associated Fibroblasts in the Bone Marrow Prevents Resistance to CART-Cell Therapy in
713 Multiple Myeloma. *Blood*, (2022).
714 24. M. Tuncel, Thyroid Stimulating Hormone Receptor. *Mol Imaging Radionucl Ther* **26**, 87-
715 91 (2017).
716 25. C. W. Rowe, J. W. Paul, C. Gedye, J. M. Tolosa, C. Bendinelli, S. McGrath, R. Smith,

717 Targeting the TSH receptor in thyroid cancer. *Endocr Relat Cancer* **24**, R191-R202 (2017).
718 26. P. Carayon, C. Thomas-Morvan, E. Castanas, M. Tubiana, Human thyroid cancer:
719 membrane thyrotropin binding and adenylate cyclase activity. *J Clin Endocrinol Metab* **51**,
720 915-920 (1980).
721 27. T. F. Davies, R. Latif, Targeting the thyroid-stimulating hormone receptor with small
722 molecule ligands and antibodies. *Expert Opin Ther Targets* **19**, 835-847 (2015).
723 28. O. ElMokh, V. Taelman, P. Radojewski, M. A. Roelli, A. Stoss, R. A. Dumont, M. S.
724 Dettmer, W. A. Phillips, M. A. Walter, R. P. Charles, MEK Inhibition Induces Therapeutic
725 Iodine Uptake in a Murine Model of Anaplastic Thyroid Cancer. *J Nucl Med* **60**, 917-923
726 (2019).
727 29. D. Liu, S. Hu, P. Hou, D. Jiang, S. Condouris, M. Xing, Suppression of BRAF/MEK/MAP
728 kinase pathway restores expression of iodide-metabolizing genes in thyroid cells
729 expressing the V600E BRAF mutant. *Clin Cancer Res* **13**, 1341-1349 (2007).
730 30. A. L. Ho, R. K. Grewal, R. Leboeuf, E. J. Sherman, D. G. Pfister, D. Deandreis, K. S.
731 Pentlow, P. B. Zanzonico, S. Haque, S. Gavane, R. A. Ghossein, J. C. Ricarte-Filho, J. M.
732 Dominguez, R. Shen, R. M. Tuttle, S. M. Larson, J. A. Fagin, Selumetinib-enhanced
733 radioiodine uptake in advanced thyroid cancer. *N Engl J Med* **368**, 623-632 (2013).
734 31. D. N. Hayes, A. S. Lucas, T. Tanvetyanon, M. K. Krzyzanowska, C. H. Chung, B. A.
735 Murphy, J. Gilbert, R. Mehra, D. T. Moore, A. Sheikh, J. Hoskins, M. C. Hayward, N. Zhao,
736 W. O'Connor, K. E. Weck, R. B. Cohen, E. E. Cohen, Phase II efficacy and
737 pharmacogenomic study of Selumetinib (AZD6244; ARRY-142886) in iodine-131
738 refractory papillary thyroid carcinoma with or without follicular elements. *Clin Cancer Res*
739 **18**, 2056-2065 (2012).
740 32. I. Landa, N. Pozdeyev, C. Korch, L. A. Marlow, R. C. Smallridge, J. A. Copland, Y. C.
741 Henderson, S. Y. Lai, G. L. Clayman, N. Onoda, A. C. Tan, M. E. R. Garcia-Rendueles, J.
742 A. Knauf, B. R. Haugen, J. A. Fagin, R. E. Schweppe, Comprehensive Genetic

743 Characterization of Human Thyroid Cancer Cell Lines: A Validated Panel for Preclinical
744 Studies. *Clin Cancer Res* **25**, 3141-3151 (2019).
745 33. J. C. Ricarte-Filho, M. Ryder, D. A. Chitale, M. Rivera, A. Heguy, M. Ladanyi, M.
746 Janakiraman, D. Solit, J. A. Knauf, R. M. Tuttle, R. A. Ghossein, J. A. Fagin, Mutational
747 profile of advanced primary and metastatic radioactive iodine-refractory thyroid cancers
748 reveals distinct pathogenetic roles for BRAF, PIK3CA, and AKT1. *Cancer Res* **69**, 4885-
749 4893 (2009).
750 34. J. A. Knauf, J. A. Fagin, Role of MAPK pathway oncoproteins in thyroid cancer
751 pathogenesis and as drug targets. *Curr Opin Cell Biol* **21**, 296-303 (2009).
752 35. M. Uhlen, L. Fagerberg, B. M. Hallstrom, C. Lindskog, P. Oksvold, A. Mardinoglu, A.
753 Sivertsson, C. Kampf, E. Sjostedt, A. Asplund, I. Olsson, K. Edlund, E. Lundberg, S.
754 Navani, C. A. Szigyarto, J. Odeberg, D. Djureinovic, J. O. Takanen, S. Hober, T. Alm, P.
755 H. Edqvist, H. Berling, H. Tegel, J. Mulder, J. Rockberg, P. Nilsson, J. M. Schwenk, M.
756 Hamsten, K. von Feilitzen, M. Forsberg, L. Persson, F. Johansson, M. Zwahlen, G. von
757 Heijne, J. Nielsen, F. Ponten, Proteomics. Tissue-based map of the human proteome.
758 *Science* **347**, 1260419 (2015).
759 36. W. C. van Staveren, D. W. Solís, L. Delys, L. Duprez, G. Andry, B. Franc, G. Thomas, F.
760 Libert, J. E. Dumont, V. Detours, C. Maenhaut, Human thyroid tumor cell lines derived
761 from different tumor types present a common dedifferentiated phenotype. *Cancer Res* **67**,
762 8113-8120 (2007).
763 37. T. Pilli, K. V. Prasad, S. Jayarama, F. Pacini, B. S. Prabhakar, Potential utility and
764 limitations of thyroid cancer cell lines as models for studying thyroid cancer. *Thyroid* **19**,
765 1333-1342 (2009).
766 38. H. Li, X. Zhou, G. Wang, D. Hua, S. Li, T. Xu, M. Dong, X. Cui, X. Yang, Y. Wu, M. Cai,
767 X. Liao, T. Zhang, Z. Yang, Y. Du, X. Li, CAR-T Cells Targeting TSHR Demonstrate Safety
768 and Potent Preclinical Activity Against Differentiated Thyroid Cancer. *J Clin Endocrinol*

769 *Metab* **107**, 1110-1126 (2022).
770 39. A. M. Meireles, A. Preto, A. S. Rocha, A. P. Rebocho, V. Máximo, I. Pereira-Castro, S.
771 Moreira, T. Feijão, T. Botelho, R. Marques, V. Trovisco, L. Cirnes, C. Alves, S. Velho, P.
772 Soares, M. Sobrinho-Simões, Molecular and genotypic characterization of human thyroid
773 follicular cell carcinoma-derived cell lines. *Thyroid* **17**, 707-715 (2007).
774 40. C. M. Stewart, E. L. Siegler, R. L. Sakemura, M. J. Cox, T. Huynh, B. Kimball, L. Mai, I.
775 Can, C. Manriquez Roman, K. Yun, O. Sirpilla, J. H. Girsch, E. Ogbodo, W. Mohammed
776 Ismail, A. Gaspar-Maia, J. Budka, J. Kim, N. Scholler, M. Mattie, S. Filosto, S. S.
777 Kenderian, IL-4 drives exhaustion of CD8(+) CART cells. *Nat Commun* **15**, 7921 (2024).
778 41. T. Liu, Q. Men, X. Su, W. Chen, L. Zou, Q. Li, M. Song, D. Ouyang, Y. Chen, Z. Li, X. Fu,
779 A. Yang, Downregulated expression of TSHR is associated with distant metastasis in
780 thyroid cancer. *Oncol Lett* **14**, 7506-7512 (2017).
781 42. M. D'Agostino, M. Sponziello, C. Puppin, M. Celano, V. Maggisano, F. Baldan, M. Biffoni,
782 S. Bulotta, C. Durante, S. Filetti, G. Damante, D. Russo, Different expression of TSH
783 receptor and NIS genes in thyroid cancer: role of epigenetics. *J Mol Endocrinol* **52**, 121-
784 131 (2014).
785 43. J. A. Fagin, S. A. Wells, Jr., Biologic and Clinical Perspectives on Thyroid Cancer. *N Engl*
786 *J Med* **375**, 2307 (2016).
787 44. N. Jin, T. Jiang, D. M. Rosen, B. D. Nelkin, D. W. Ball, Dual inhibition of mitogen-activated
788 protein kinase kinase and mammalian target of rapamycin in differentiated and anaplastic
789 thyroid cancer. *J Clin Endocrinol Metab* **94**, 4107-4112 (2009).
790 45. D. Chakravarty, E. Santos, M. Ryder, J. A. Knauf, X. H. Liao, B. L. West, G. Bollag, R.
791 Kolesnick, T. H. Thin, N. Rosen, P. Zanzonico, S. M. Larson, S. Refetoff, R. Ghossein, J.
792 A. Fagin, Small-molecule MAPK inhibitors restore radioiodine incorporation in mouse
793 thyroid cancers with conditional BRAF activation. *J Clin Invest* **121**, 4700-4711 (2011).
794 46. V. Subbiah, R. J. Kreitman, Z. A. Wainberg, J. Y. Cho, J. H. M. Schellens, J. C. Soria, P.

795 Y. Wen, C. Zielinski, M. E. Cabanillas, G. Urbanowitz, B. Mookerjee, D. Wang, F.
796 Rangwala, B. Keam, Dabrafenib and Trametinib Treatment in Patients With Locally
797 Advanced or Metastatic BRAF V600-Mutant Anaplastic Thyroid Cancer. *J Clin Oncol* **36**,
798 7-13 (2018).
799 47. I. M. Wakelkamp, O. Bakker, L. Baldeschi, W. M. Wiersinga, M. F. Prummel, TSH-R
800 expression and cytokine profile in orbital tissue of active vs. inactive Graves'
801 ophthalmopathy patients. *Clin Endocrinol (Oxf)* **58**, 280-287 (2003).
802 48. R. S. Bahn, TSH receptor expression in orbital tissue and its role in the pathogenesis of
803 Graves' ophthalmopathy. *J Endocrinol Invest* **27**, 216-220 (2004).
804 49. X. Cui, F. Wang, C. Liu, A review of TSHR- and IGF-1R-related pathogenesis and
805 treatment of Graves' orbitopathy. *Front Immunol* **14**, 1062045 (2023).
806 50. H. Y. Choi, H. Jeon, J. W. Yang, J. H. Ahn, J. H. Jung, Thyroid-Stimulating Hormone
807 Receptor Expression on Primary Cultured Human Extraocular Muscle Myoblasts. *Curr*
808 *Eye Res* **43**, 1484-1488 (2018).
809 51. Y. Lu, S. J. Atkins, R. Fernando, A. Trierweiler, T. Mester, A. B. D. Grisolia, P. Mou, P.
810 Novaes, T. J. Smith, CD34- Orbital Fibroblasts From Patients With Thyroid-Associated
811 Ophthalmopathy Modulate TNF-α Expression in CD34+ Fibroblasts and Fibrocytes. *Invest*
812 *Ophthalmol Vis Sci* **59**, 2615-2622 (2018).
813 52. J. Furmaniak, J. Sanders, P. Sanders, Y. Li, B. Rees Smith, TSH receptor specific
814 monoclonal autoantibody K1-70TM targeting of the TSH receptor in subjects with Graves'
815 disease and Graves' orbitopathy—Results from a phase I clinical trial. *Clinical*
816 *Endocrinology* **96**, 878-887 (2022).
817 53. M. Ryder, M. Wentworth, A. Algeciras-Schimnich, J. C. Morris, J. Garrity, J. Sanders, S.
818 Young, P. Sanders, J. Furmaniak, B. Rees Smith, Blocking the Thyrotropin Receptor with
819 K1-70 in a Patient with Follicular Thyroid Cancer, Graves' Disease, and Graves'
820 Ophthalmopathy. *Thyroid* **31**, 1597-1602 (2021).

821 54. I. M. Min, E. Shevlin, Y. Vedvyas, M. Zaman, B. Wyrwas, T. Scognamiglio, M. D. Moore,
822 W. Wang, S. Park, S. Park, S. Panjwani, K. D. Gray, A. B. Tassler, R. Zarnegar, T. J.
823 Fahey, 3rd, M. M. Jin, CAR T Therapy Targeting ICAM-1 Eliminates Advanced Human
824 Thyroid Tumors. *Clin Cancer Res* **23**, 7569-7583 (2017).
825 55. V. G. Bhoj, L. Li, K. Parvathaneni, Z. Zhang, S. Kacir, D. Arhontoulis, K. Zhou, B.
826 McGettigan-Croce, S. Nunez-Cruz, G. Gulendran, A. C. Boesteanu, L. Johnson, M. D.
827 Feldman, E. Radaelli, K. Mansfield, M. Nasrallah, R. S. Goydel, H. Peng, C. Rader, M. C.
828 Milone, D. L. Siegel, Adoptive T cell immunotherapy for medullary thyroid carcinoma
829 targeting GDNF family receptor alpha 4. *Mol Ther Oncolytics* **20**, 387-398 (2021).
830 56. L. Xiao, X. C. Liu, K. S. Zhou, Y. Liu, Y. Huang, C. F. Pu, Z. Y. Cao, R. H. Zhu, H. Y. Tang,
831 Z. P. Huang, H. Yang, X. Huang, Y. P. Song, R. B. Liu, Z. Wu, V. Lu, CoupledCAR
832 technology for treating thyroid cancer. *Journal of Clinical Oncology* **39**, (2021).
833 57. J. Ding, D. Li, X. Liu, H. Hei, B. Sun, D. Zhou, K. Zhou, Y. Song, Chimeric antigen receptor
834 T-cell therapy for relapsed and refractory thyroid cancer. *Exp Hematol Oncol* **11**, 59
835 (2022).
836 58. L. Liu, P. A. Mayes, S. Eastman, H. Shi, S. Yadavilli, T. Zhang, J. Yang, L. Seestaller-
837 Wehr, S. Y. Zhang, C. Hopson, L. Tsvetkov, J. Jing, S. Zhang, J. Smothers, A. Hoos, The
838 BRAF and MEK Inhibitors Dabrafenib and Trametinib: Effects on Immune Function and in
839 Combination with Immunomodulatory Antibodies Targeting PD-1, PD-L1, and CTLA-4.
840 *Clin Cancer Res* **21**, 1639-1651 (2015).
841 59. C. Liu, W. Peng, C. Xu, Y. Lou, M. Zhang, J. A. Wargo, J. Q. Chen, H. S. Li, S. S.
842 Watowich, Y. Yang, D. Tompers Frederick, Z. A. Cooper, R. M. Mbofung, M. Whittington,
843 K. T. Flaherty, S. E. Woodman, M. A. Davies, L. G. Radvanyi, W. W. Overwijk, G. Lizée,
844 P. Hwu, BRAF inhibition increases tumor infiltration by T cells and enhances the antitumor
845 activity of adoptive immunotherapy in mice. *Clin Cancer Res* **19**, 393-403 (2013).
846 60. V. Verma, N. Jafarzadeh, S. Boi, S. Kundu, Z. Jiang, Y. Fan, J. Lopez, R. Nandre, P. Zeng,

847 F. Alolaqi, S. Ahmad, P. Gaur, S. T. Barry, V. E. Valge-Archer, P. D. Smith, J. Banchereau,
848 M. Mkrtichyan, B. Youngblood, P. C. Rodriguez, S. Gupta, S. N. Khleif, MEK inhibition
849 reprograms CD8(+) T lymphocytes into memory stem cells with potent antitumor effects.
850 *Nat Immunol* **22**, 53-66 (2021).
851 61. T. Mitra, J. Rahman, M. Hwee, R. J. Jesus Faustino Ramos, H. Liu, T. Hartman, J. Cross,
852 M. de Jesus, M. Huse, V. Longo, P. Zanzonico, S. A. Vardhana, MEK-dependent
853 bioenergetic demand drives terminal CD8⁺ T cell exhaustion. *bioRxiv*,
854 2025.2004.2030.651453 (2025).
855 62. T. Gargett, C. K. Fraser, G. Dotti, E. S. Yvon, M. P. Brown, BRAF and MEK inhibition
856 variably affect GD2-specific chimeric antigen receptor (CAR) T-cell function in vitro. *J*
857 *Immunother* **38**, 12-23 (2015).
858 63. A. Tomida, S. Yagyu, K. Nakamura, H. Kubo, K. Yamashima, Y. Nakazawa, H. Hosoi, T.
859 Iehara, Inhibition of MEK pathway enhances the antitumor efficacy of chimeric antigen
860 receptor T cells against neuroblastoma. *Cancer Sci* **112**, 4026-4036 (2021).
861 64. J. Dörrie, L. Babalija, S. Hoyer, K. F. Gerer, G. Schuler, L. Heinzerling, N. Schaft, BRAF
862 and MEK Inhibitors Influence the Function of Reprogrammed T Cells: Consequences for
863 Adoptive T-Cell Therapy. *Int J Mol Sci* **19**, (2018).
864 65. X. Wang, X. Tao, P. Chen, P. Jiang, W. Li, H. Chang, C. Wei, X. Lai, H. Zhang, Y. Pan, L.
865 Ding, Z. Liang, J. Cui, M. Shao, X. Teng, T. Gu, J. Wei, D. Kong, X. Si, Y. Han, H. Fu, Y.
866 Lin, J. Yu, X. Li, D. Wang, Y. Hu, P. Qian, H. Huang, MEK inhibition prevents CAR-T cell
867 exhaustion and differentiation via downregulation of c-Fos and JunB. *Signal Transduct*
868 *Target Ther* **9**, 293 (2024).
869 66. L. A. Marlow, S. D. Rohl, J. L. Miller, J. A. Knauf, J. A. Fagin, M. Ryder, D. Milosevic, B.
870 C. Netzel, S. K. Grebe, H. V. Reddi, R. C. Smallridge, J. A. Copland, Methodology, Criteria,
871 and Characterization of Patient-Matched Thyroid Cell Lines and Patient-Derived Tumor
872 Xenografts. *J Clin Endocrinol Metab* **103**, 3169-3182 (2018).

873 67. A. Zielke, S. Tezelman, G. H. Jossart, M. Wong, A. E. Siperstein, Q. Y. Duh, O. H. Clark,
874 Establishment of a highly differentiated thyroid cancer cell line of Hurthle cell origin.
875 *Thyroid* **8**, 475-483 (1998).
876 68. R. M. Sterner, R. Sakemura, M. J. Cox, N. Yang, R. H. Khadka, C. L. Forsman, M. J.
877 Hansen, F. Jin, K. Ayasoufi, M. Hefazi, K. J. Schick, D. K. Walters, O. Ahmed, D. Chappell,
878 T. Sahmoud, C. Durrant, W. K. Nevala, M. M. Patnaik, L. R. Pease, K. E. Hedin, N. E.
879 Kay, A. J. Johnson, S. S. Kenderian, GM-CSF inhibition reduces cytokine release
880 syndrome and neuroinflammation but enhances CAR-T cell function in xenografts. *Blood*
881 **133**, 697-709 (2019).
882 69. A. B. Dietz, P. A. Bulur, R. L. Emery, J. L. Winters, D. E. Epps, A. C. Zubair, S. Vuk-
883 Pavlovic, A novel source of viable peripheral blood mononuclear cells from leukoreduction
884 system chambers. *Transfusion* **46**, 2083-2089 (2006).
885 70. J. Sanders, R. N. Miguel, J. Furmaniak, B. R. Smith, TSH receptor monoclonal antibodies
886 with agonist, antagonist, and inverse agonist activities. *Methods Enzymol* **485**, 393-420
887 (2010).
888 71. R. L. Sakemura, M. Hefazi, M. J. Cox, E. L. Siegler, S. Sinha, M. J. Hansen, C. M. Stewart,
889 J. M. Feigin, C. Manriquez Roman, K. J. Schick, I. Can, E. E. Tapper, P. Horvei, M. M.
890 Adada, E. D. Bezerra, L. A. Kankeu Fonkoua, M. W. Ruff, C. L. Forsman, W. K. Nevala,
891 J. C. Boysen, R. C. Tschumper, C. L. Grand, K. R. Kuchimanchi, L. Mouritsen, J. M.
892 Foulks, S. L. Warner, T. G. Call, S. A. Parikh, W. Ding, N. E. Kay, S. S. Kenderian, AXL
893 Inhibition Improves the Antitumor Activity of Chimeric Antigen Receptor T Cells. *Cancer*
894 *Immunol Res* **11**, 1222-1236 (2023).
895 72. M. J. Cox, C. Manriquez Roman, E. E. Tapper, E. L. Siegler, D. Chappell, C. Durrant, O.
896 Ahmed, S. Sinha, R. Mwangi, N. S. Scott, M. Hefazi, K. J. Schick, P. Horvei, M. W. Ruff,
897 I. Can, M. Adada, E. Bezerra, L. A. Kankeu Fonkoua, S. A. Parikh, N. E. Kay, R.
898 Sakemura, S. S. Kenderian, GM-CSF disruption in CART cells modulates T cell activation

899 and enhances CART cell anti-tumor activity. *Leukemia*, (2022).

900 73. M. J. Cox, F. Lucien, R. Sakemura, J. C. Boysen, Y. Kim, P. Horvei, C. Manriquez Roman,
901 M. J. Hansen, E. E. Tapper, E. L. Siegler, C. Forsman, S. B. Crotts, K. J. Schick, M. Hefazi,
902 M. W. Ruff, I. Can, M. Adada, E. Bezerra, L. A. Kankeu Fonkoua, W. K. Nevala, E. Braggio,
903 W. Ding, S. A. Parikh, N. E. Kay, S. S. Kenderian, Leukemic extracellular vesicles induce
904 chimeric antigen receptor T cell dysfunction in chronic lymphocytic leukemia. *Mol Ther* **29**,
905 1529-1540 (2021).

906 74. R. Sakemura, A. Bansal, E. L. Siegler, M. Hefazi, N. Yang, R. H. Khadka, A. N. Newsom,
907 M. J. Hansen, M. J. Cox, C. Manriquez Roman, K. J. Schick, I. Can, E. E. Tapper, W. K.
908 Nevala, M. M. Adada, E. D. Bezerra, L. A. Kankeu Fonkoua, P. Horvei, M. W. Ruff, S. A.
909 Parikh, M. K. Pandey, T. R. DeGrado, L. Suksanpaisan, N. E. Kay, K. W. Peng, S. J.
910 Russell, S. S. Kenderian, Development of a Clinically Relevant Reporter for Chimeric
911 Antigen Receptor T-cell Expansion, Trafficking, and Toxicity. *Cancer Immunol Res* **9**,
912 1035-1046 (2021).

913

914

915 **FIGURES**

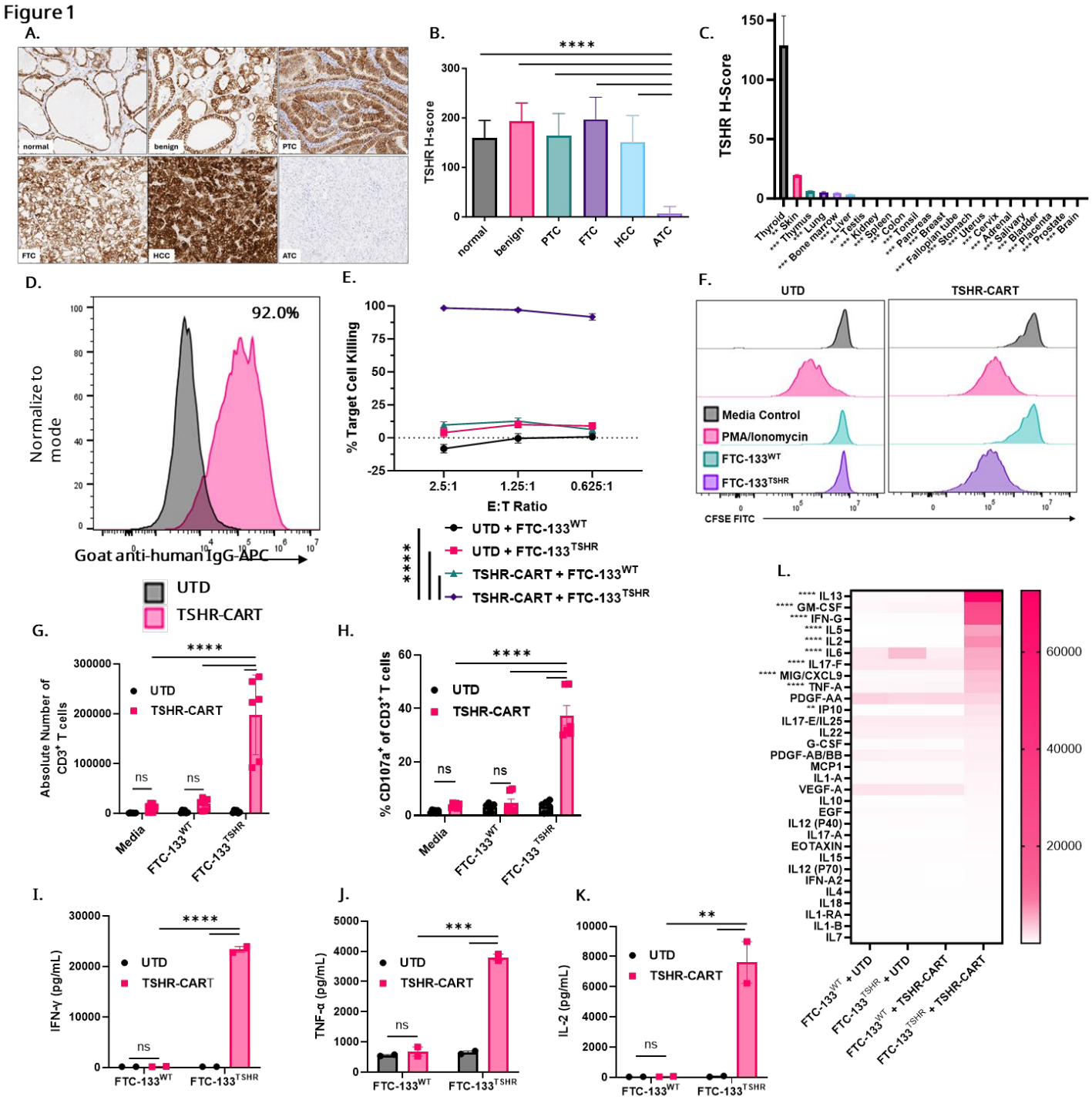

916 **Figure 1. TSHR is a rational target for CART cell therapy, and TSHR-CART cells**
917 **demonstrate antigen-specific effector functions *in vitro*. A)** Representative IHC staining
918 shows TSHR expression across normal, benign, and malignant thyroid tissues. PTC: papillary

919 thyroid cancer; FTC: follicular thyroid cancer; HCC: Hurthle cell carcinoma; ATC: anaplastic
920 thyroid cancer. **B)** H-score quantitation of TSHR expression is shown. H-scores provided are
921 based on 0 – 3 IHC scoring and percentage of total areas each score (0x%0 + 1x%1 + 2x%2 +
922 3x%3 = H Score; 0 – 300 range with statistical analysis (mean and SEM; ****p < 0.0001, one-way
923 ANOVA; normal n = 11, benign n = 9, PTC n = 11, FTC n = 9, HCC n = 37, ATC n = 10). **C)** H-
924 score quantification of normal human tissue stained with TSHR (mean and SEM; **p < 0.01, ***p
925 < 0.001, one-way ANOVA; thyroid n = 7, all other tissues n = 2). **D)** Representative histogram
926 shows CAR expression on TSHR-CART cells as determined by flow cytometry. UTD T cells were
927 used as a negative control. **E)** Luciferase^{+} TSHR^{+} or TSHR^{-} FTC-133 target cells were co-cultured
928 with either UTD or TSHR-CART cells at varying effector-to-target ratios, and cytotoxicity was
929 measured via bioluminescence after 48 hours (mean and SEM; ***p < 0.001, ****p < 0.0001, two-
930 way ANOVA; 3 biological replicates). **F-G)** CFSE-labeled UTD or TSHR-CART cells were co-
931 cocultured with media alone (negative control), PMA/ionomycin (positive control), or TSHR^{+} or
932 TSHR^{-} FTC-133 target cells. After five days, T cell proliferation was assessed by flow cytometry
933 using CFSE staining (F) or absolute counts of CD3^{+} cells (G) (mean and SEM; ****p < 0.0001,
934 two-way ANOVA; 3 biological replicates). **H)** UTD or TSHR-CART cells were-cocultured with
935 TSHR^{+} FTC-133 target cells at a 1:5 ratio for four hours, and degranulation was then assessed
936 by flow cytometry of CD3^{+} CD107a^{+} cells (mean and SEM; ****p < 0.0001, two-way ANOVA; 2
937 biological replicates). **I-K)** UTD or TSHR-CART cells were-cocultured with TSHR^{-} or TSHR^{+} FTC-
938 133 target cells at a 1:1 ratio for three days, and supernatants were analyzed for human cytokines
939 via a 38-multiplex assay (mean and SEM; **p < 0.01, ***p < 0.001, ****p < 0.0001, two-way
940 ANOVA; 2 biological replicates). **L)** Heat map of additional analytes from the 38-plex assay
941 (median; **p < 0.01, ****p < 0.0001, two-way ANOVA; 2 biological replicates).
942

943 Figure 2

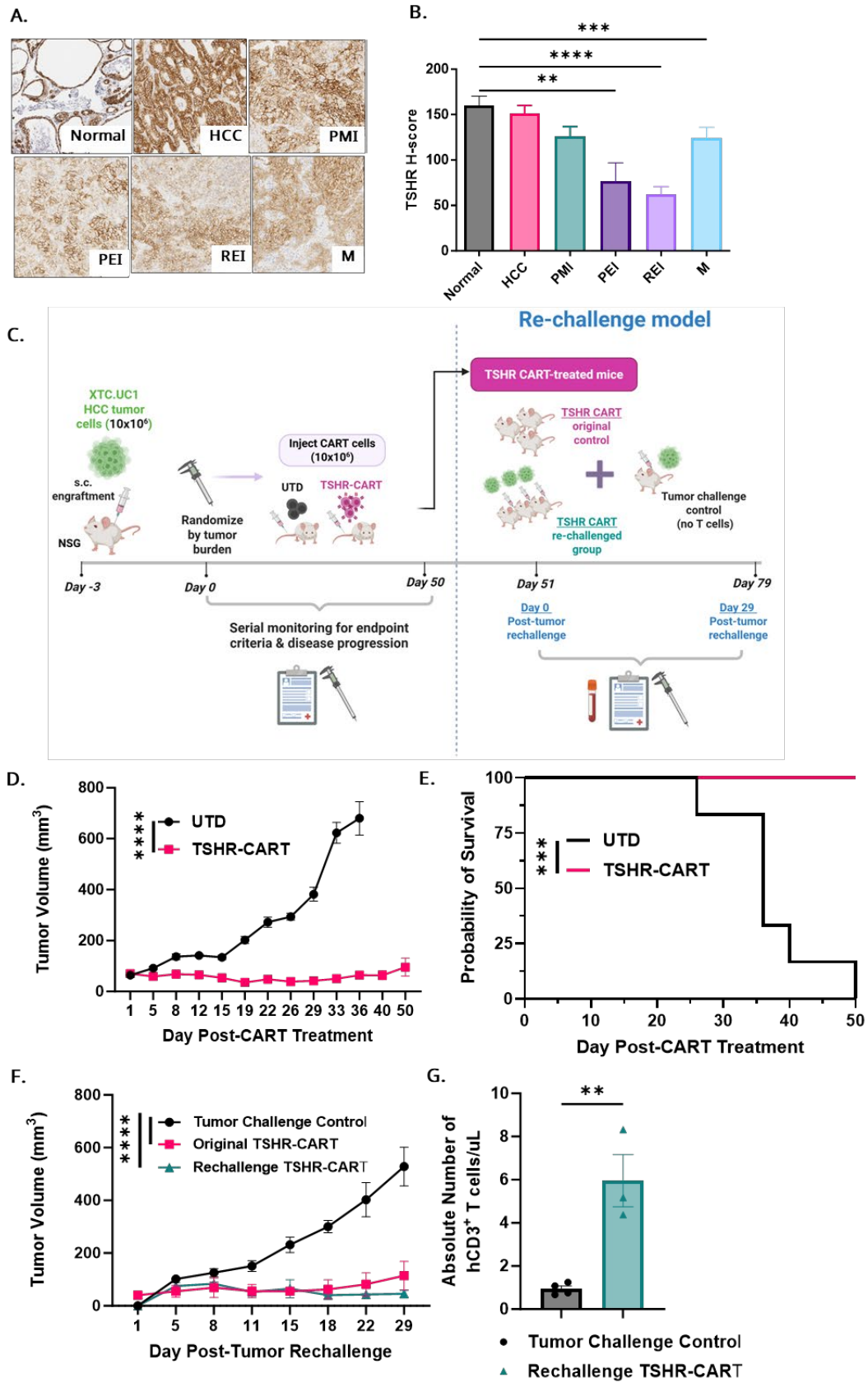
A.
Normal
HCC
PMI
PEI
REI
M
B.
***
****
**
TSHR H-score
200
150
100
50
0
Normal
HCC
PMI
PEI
REI
M
C.
Re-challenge model
TSHR CART-treated mice
XTC.UC1 HCC tumor cells (10x10⁶)
s.c. engraftment
NSG
Randomize by tumor burden
Inject CART cells (10x10⁶)
UTD
TSHR-CART
TSHR CART original control
TSHR CART re-challenged group
Tumor challenge control (no T cells)
Day -3
Day 0
Day 50
Day 51
Day 79
Serial monitoring for endpoint criteria & disease progression
Day 0 Post-tumor rechallenge
Day 29 Post-tumor rechallenge
D.
Tumor Volume (mm³)
800
600
400
200
0
****
UTD
TSHR-CART
1 5 8 12 15 19 22 26 29 33 36 40 50
Day Post-CART Treatment
E.
Probability of Survival
100
75
50
25
0
**
UTD
TSHR-CART
0 10 20 30 40 50
Day Post-CART Treatment
F.
Tumor Volume (mm³)
800
600
400
200
0
****
Tumor Challenge Control
Original TSHR-CART
Rechallenge TSHR-CART
1 5 8 11 15 18 22 29
Day Post-Tumor Rechallenge
G.
Absolute Number of hCD3⁺ T cells/uL
10
8
6
4
2
0
**
Tumor Challenge Control
Rechallenge TSHR-CART

944 **Figure 2. TSHR-CART cells exhibit potent antitumor activity in vivo against Hurthle cell**
945 **carcinoma. A)** Representative IHC staining of TSHR expression across normal and HCC tissues.
946 Hurthle cell carcinoma: HCC; primary tumor with minimal invasion: PMI; primary tumor with
947 extensive invasion: PEI; recurrent tumor with extensive invasion: REI; metastatic tumors: M. **B)**
948 TSHR expression was quantified using H-Score (based on 0 – 300 IHC scoring and percentage
949 of total areas each score, 0 – 300 range with statistical analysis) (mean and SEM; **p < 0.01, ***p
950 < 0.001, ****p <0.0001, one-way ANOVA. Normal n=11, HCC n=37, PMI n=26, PEI n=11, REI
951 n=34, M n=16). **C)** Experimental schema of a HCC xenograft model. NSG mice were
952 subcutaneously engrafted with $TSHR^+$ XTC.UC1 thyroid cancer cells in Matrigel. Three days later,
953 after engraftment was confirmed, mice were randomized according to tumor volume to receive
954 either UTD (10×10^6) or TSHR-CART cells (10×10^6) intravenously. Mice were monitored for
955 well-being, tumor volume, and overall survival. At day 51, mice treated with TSHR-CART cells
956 which achieved complete remission were rechallenged subcutaneously with XCT.UC1 cells in the
957 opposite flank. Additionally, an untreated group was engrafted with XCT.UC1 cells and included
958 as a negative control. Mice were monitored for well-being, tumor volume, T cell expansion, and
959 overall survival. **D)** Tumor volume was assessed via serial caliper measurements (mean and
960 SEM; ****p < 0.0001, two-way ANOVA; n=6 mice per group). **E)** Kaplan-Meier survival curve (***p
961 < 0.001, Log-rank test; n=6 mice per group). **F)** Tumor volume as assessed by serial caliper
962 measurements (mean and SEM; ****p < 0.0001, two-way ANOVA; n=6 mice per group). **G)**
963 Peripheral blood was collected 21 days after tumor rechallenge and assessed by flow cytometry
964 using absolute counts of $hCD3^+$ cells (mean and SEM; **p < 0.01, two-tailed unpaired t-test; n =
965 3 mice per group).
966
967

Figure 3

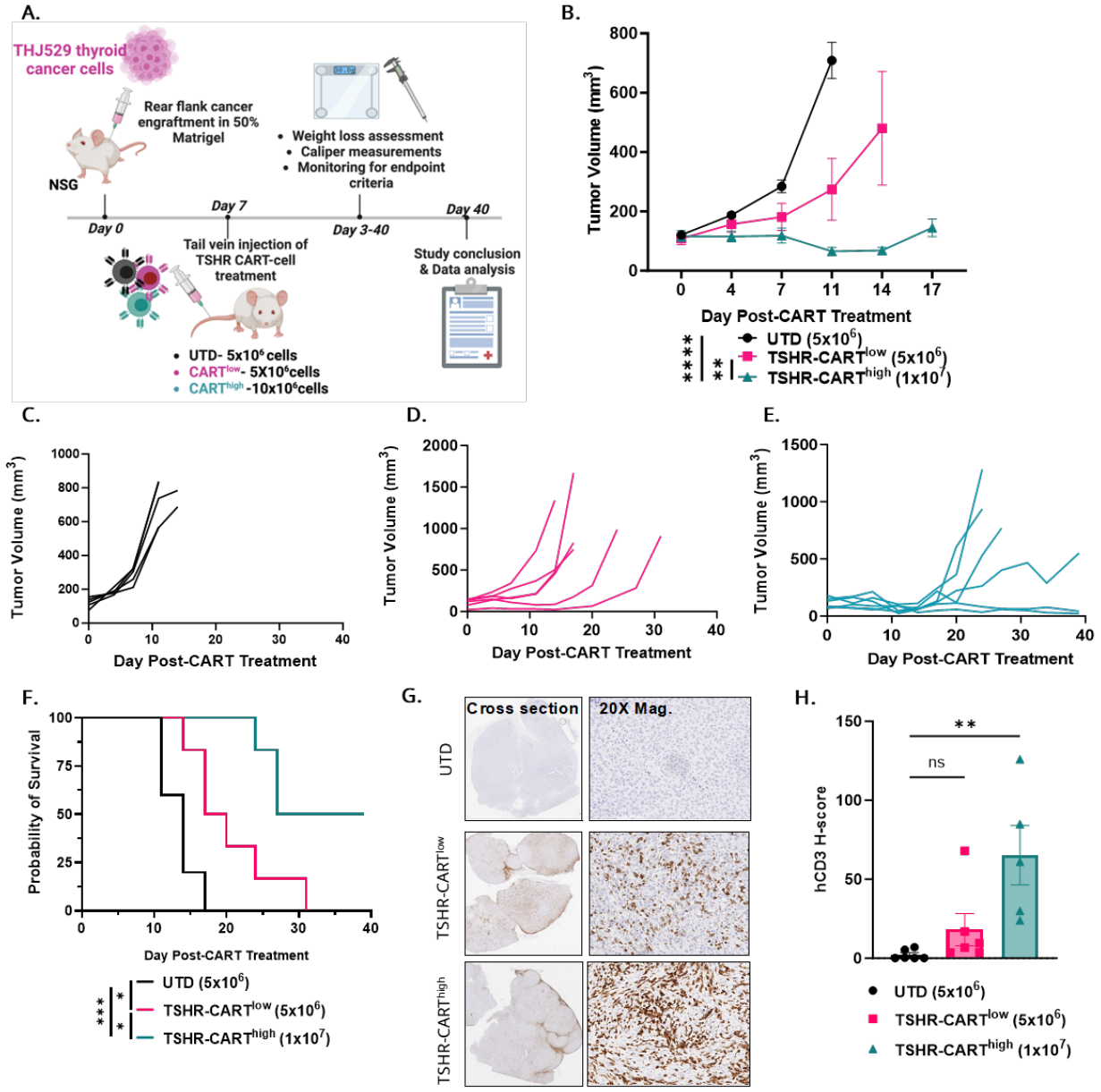

Figure 3. TSHR-CART cells exhibit dose-dependent antitumor activity in PDX models of TSHR⁺ PDTC. A) Experimental schema of a PDTC xenograft model. NSG mice were subcutaneously engrafted with TSHR^{+} THJ-529 thyroid cancer cells in Matrigel. One week later, after engraftment was confirmed, mice were randomized according to tumor volume and received either UTD (5 x 10^{6}) or TSHR-CART cells (5 x 10^{6} or 1 x 10^{7}) intravenously. Mice were monitored for well-being, tumor volume, and overall survival. **B)** Tumor volume was assessed via serial

974 caliper measurements (mean and SEM; **$p < 0.01$, ****$p < 0.0001$, two-way ANOVA; n=5-6 mice
975 per group). **C-E)** Individual tumor growth curves are shown for each treatment group, including
976 UTD (**C**), TSHR-CART^{low} (**D**), and TSHR-CART^{high} (**E**). N = 5-6 mice/group. **F)** Kaplan-Meier
977 survival curve (*$p < 0.05$, ***$p < 0.001$, Log-rank test; n=5-6 mice per group). **G)** Representative
978 IHC staining shows human CD3 expression in thyroid tumors excised from mice in each treatment
979 group. **H)** H-score quantitation of human CD3 expression is shown. H-scores provided are based
980 on 0 – 3 IHC scoring and percentage of total areas each score (0x%0 + 1x%1 + 2x%2 + 3x%3 =
981 H Score; 0 – 300 range with statistical analysis) (mean and SEM; **$p < 0.01$, one-way ANOVA; n
982 = 5-6 mice per group).
983
984

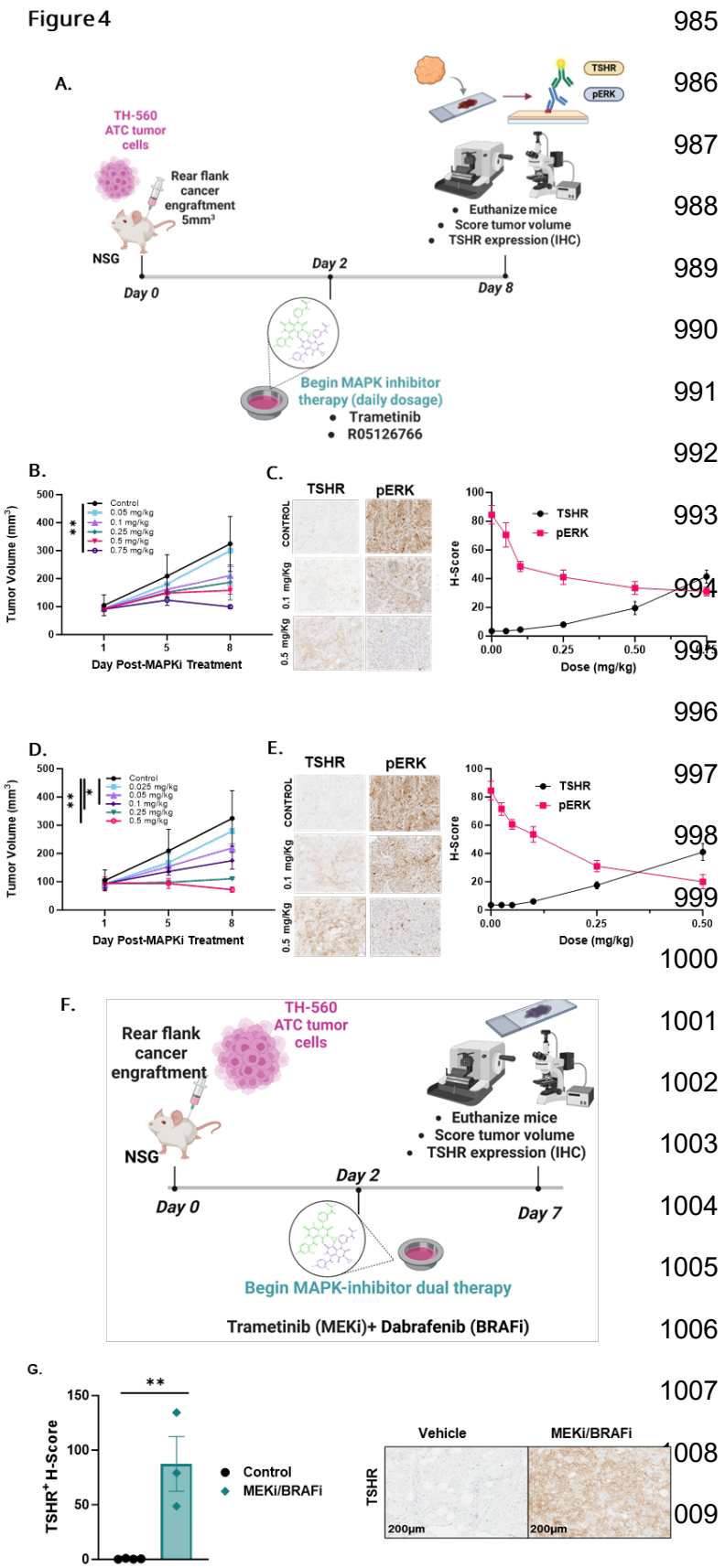

Figure 4. Treatment of ATC PDX tumors with MAPK inhibitors restores TSHR expression. A) Experimental schema of an ATC PDX model. NSG mice were subcutaneously engrafted with TH-560 ATC PDX tumors. When tumors reached approximately 100 mm^3, mice were orally treated with MAPK inhibitors daily and serially monitored for tumor volume. On day 8, mice were sacrificed, and tumors were harvested and assessed for TSHR expression by IHC. **B)** Tumor volumes were assessed via serial caliper measurements in mice treated with trametinib at the indicated doses (mean and SEM; **p < 0.01, two-way ANOVA; n=2 mice per group). **C)** Representative IHC staining (left) shows human TSHR and

1010 pERK expression in thyroid tumors excised from mice in each treatment group. H-scores (right)
1011 provided are based on 0 – 3 IHC scoring and percentage of total areas each score (0x%0 + 1x%1
1012 + 2x%2 + 3x%3 = H Score; 0 – 300 range with statistical analysis. Mean and SEM; n = 2 mice
1013 per group). **D)** Tumor volumes were assessed via serial caliper measurements in mice treated
1014 with RO5126766 at the indicated doses (mean and SEM; *p < 0.05, **p < 0.01, two-way ANOVA;
1015 n=2 mice per group). **E)** Representative IHC staining (left) and H-score quantitation (right) show
1016 human TSHR and pERK expression in thyroid tumors excised from mice in each treatment group.
1017 H-scores provided are based on 0 – 3 IHC scoring and percentage of total areas each score
1018 (0x%0 + 1x%1 + 2x%2 + 3x%3 = H Score; 0 – 300 range with statistical analysis. Mean and SEM;
1019 n = 2 mice per group). **F)** Experimental schema of an ATC PDX model. NSG mice were
1020 subcutaneously engrafted with Th-560 ATC PDX tumors. When tumors reached approximately
1021 100 mm^3, mice were orally treated with MAPK inhibitors daily and serially monitored for tumor
1022 volume. On Day 7, mice were sacrificed, and tumors were harvested and assessed for TSHR
1023 expression by IHC. **G)** Representative IHC staining (top) and H-score quantitation (bottom) show
1024 human TSHR expression in thyroid tumors excised from mice in each treatment group. H-scores
1025 provided are based on 0 – 3 IHC scoring and percentage of total areas each score (0x%0 + 1x%1
1026 + 2x%2 + 3x%3 = H Score; 0 – 300 range with statistical analysis. Mean and SEM; **p <0.01,
1027 unpaired two-tailed t-test, n = 3-4 mice per group).

Figure 5

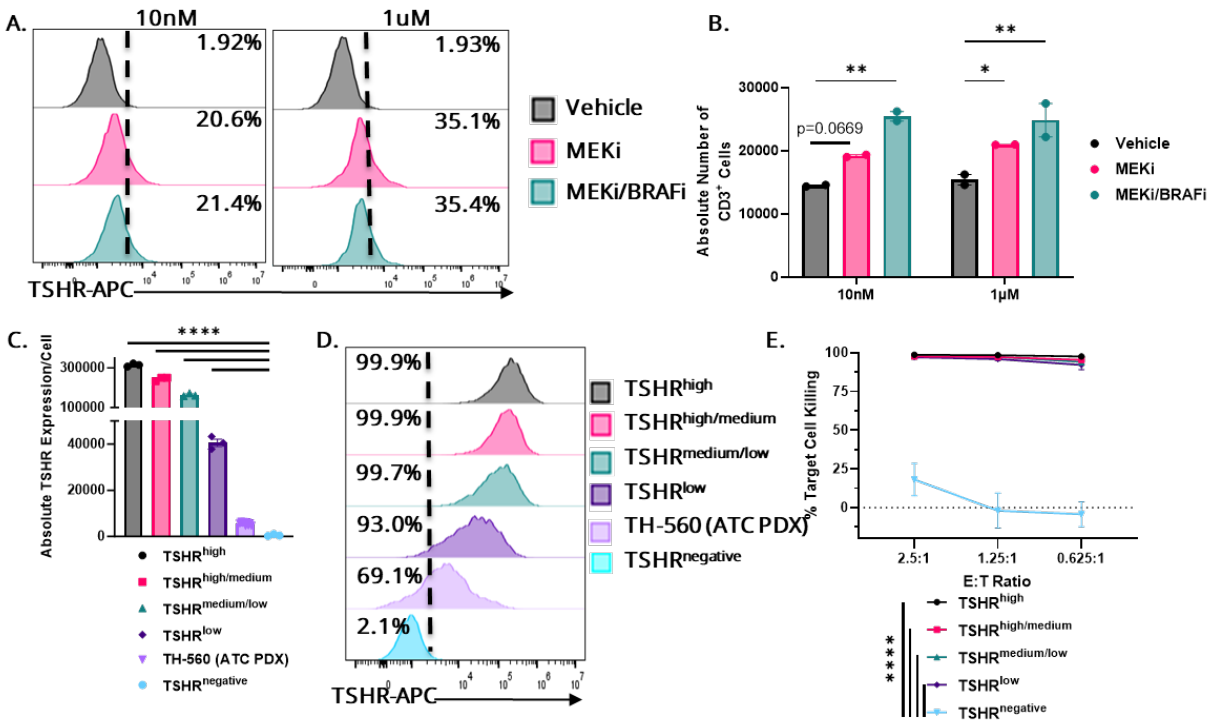

Figure 5. TSHR-CART cells are sensitive to moderate upregulation of TSHR on target cells. **A)** THJ-529 cells were cocultured with 10 nM or 1μM vehicle control, trametinib, or both trametinib and dabrafenib. After four days, THJ-529 cells were trypsinized and flowed for TSHR expression. Representative histogram shown. **B)** After four days of MAPK inhibitor co-culture, THJ-529 cells were trypsinized and plated with TSHR-CART cells at a 1:1 ratio and assessed for proliferation five days later as determined by flow cytometry of absolute number of $CD3^+$ cells (mean and SEM; *$p < 0.05$, **$p < 0.01$, two-way ANOVA; 1 biological replicate). **C)** Assessment of absolute TSHR expression levels in wildtype or lentivirally transduced $TSHR^+$ FTC-133 tumor cells and wildtype PDX tumors, as determined by flow cytometry using absolute counting beads (mean and SEM; ****$p < 0.0001$, one-way ANOVA; n= 3-9 technical replicates). **D)** Representative histogram shows different levels of TSHR expression on tumor cells as determined by flow cytometry. **E)** Percentage of killing measured via bioluminescent imaging after 48 hours of co-culture at different

1040 E:T ratios of TSHR-CART cells and luciferase$^+$ FTC-133 tumor cells expressing various levels of

1041 TSHR (mean and SEM; ****p < 0.0001, two-way ANOVA; 2 biological replicates).

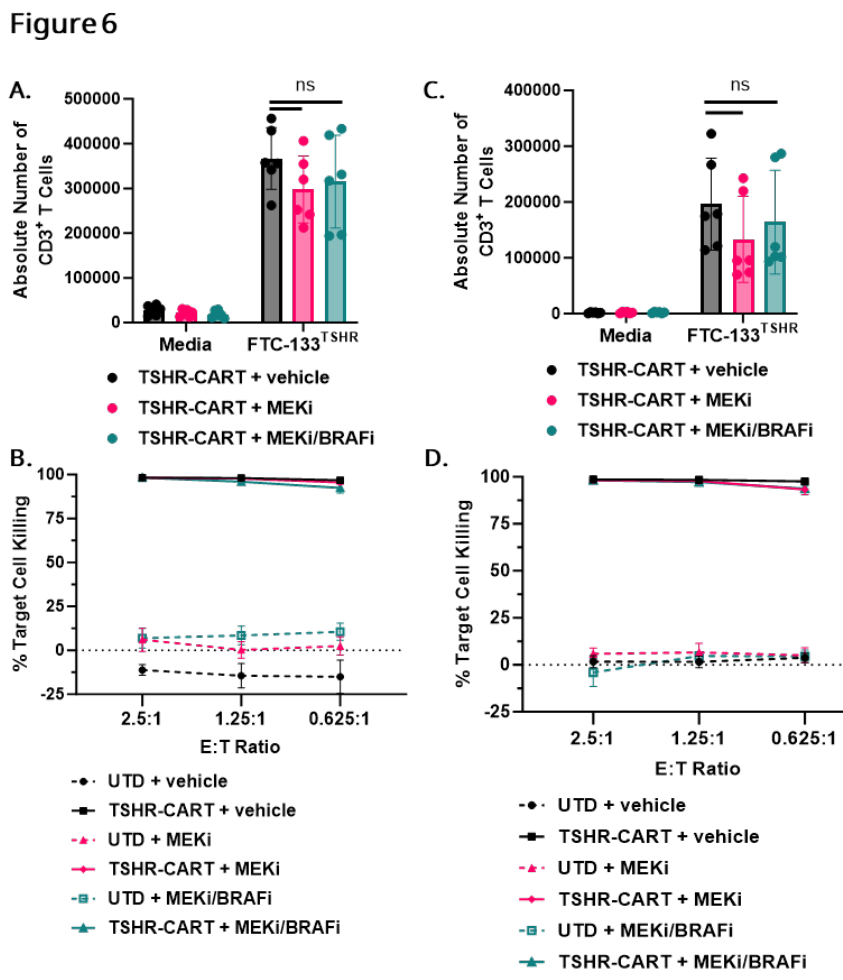

1042 **Figure 6. TSHR-**

1043 **CART effector**

1044 **functions remain**

1045 **intact after the**

1046 **addition of MAPK**

1047 **inhibitors. A)** TSHR-

1048 CART cells were co-

1049 cocultured with either

1050 media alone

1051 (negative control) or

1052 TSHR$^+$ FTC-133

1053 target cells at a 1:1

1054 ratio, along with

1055 vehicle control, 10nM

1056 trametinib, or 10nM

1057 both trametinib and dabrafenib. After five days, T cell proliferation was assessed by flow cytometry

1058 using absolute counts of CD3$^+$ cells (mean and SEM; two-way ANOVA; 2 biological replicates).

1059 **B)** TSHR-CART cells were-cocultured with luciferase$^+$ TSHR$^+$ FTC-133 target cells at various E:T

1060 ratios, along with vehicle control, 10nM trametinib, or 10nM both trametinib and dabrafenib. After

1061 48 hours, target cell killing was assessed by bioluminescence (mean and SEM; two-way ANOVA;

1062 2 biological replicates). **C-D)** In chronic stimulation assays, TSHR-CART cells were co-cocultured

1063 with either media alone (negative control) or irradiated TSHR$^+$ FTC-133 target cells at a 1:1 ratio,

1064 along with vehicle control, 10nM trametinib, or 10nM both trametinib and dabrafenib. Irradiated

target cells and MAPK inhibitor-containing media were replenished every other day for one week. Then, TSHR-CART cells were isolated with CD4 and CD8 beads and plated in proliferation (**C**) or cytotoxicity (**D**) assays as described above (mean and SEM; two-way ANOVA; 2 biological replicates).

Figure 7

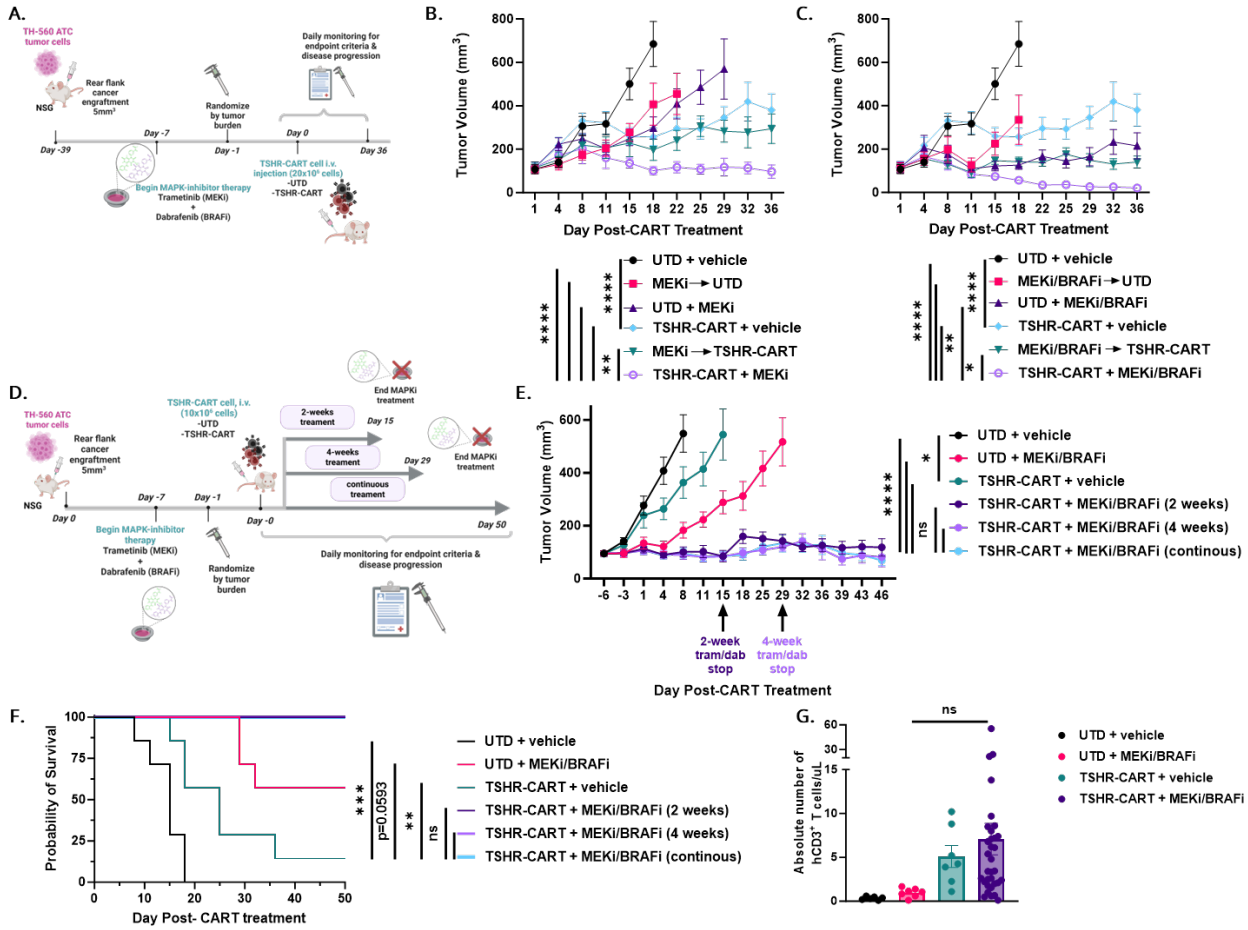

Figure 7. TSHR-CART cells show the most potent antitumor activity when combined with MAPK inhibitor administration. A) Experimental schema of an ATC PDX model. NSG mice were subcutaneously engrafted with Th-560 ATC PDX tumors. When tumors reached approximately 100 mm^3, mice were orally treated with MAPK inhibitors (0.25 mg/kg trametinib alone or with 2 mg/kg dabrafenib) daily for either seven days prior to TSHR-CART administration or concurrently (until endpoints were reached) and serially monitored for tumor volume. Mice were then randomized by tumor volume and treated with either UTD or TSHR-CART cells ($20x10^6$ i.v.).

1076 Mice were monitored for well-being and tumor volume. **B)** Tumor volumes were assessed via
1077 serial caliper measurements in mice treated with UTD or TSHR-CART with vehicle control, with
1078 7 days of trametinib, or with concurrent trametinib at the indicated doses (mean and SEM; **p <
1079 0.01, ****p < 0.0001, two-way ANOVA; n=7 mice per group). **C)** Tumor volumes were assessed
1080 via serial caliper measurements in mice treated with UTD or TSHR-CART with vehicle control,
1081 with 7 days of trametinib plus dabrafenib, or with concurrent trametinib plus dabrafenib at the
1082 indicated doses (mean and SEM; *p < 0.05, **p < 0.01, ****p < 0.0001, two-way ANOVA; n=7
1083 mice per group). **D)** Experimental schema of an ATC PDX model. NSG mice were subcutaneously
1084 engrafted with Th-560 ATC PDX tumors. When tumors reached approximately 100 mm^3, mice
1085 were orally treated with MAPK inhibitors (0.25 mg/kg trametinib plus 2 mg/kg dabrafenib) daily for
1086 seven days monitored for tumor volume. After 7 days of MAPK inhibitor treatment, mice were
1087 randomized by tumor volume to be treated with either UTD or TSHR-CART cells ($10x10^6$ i.v.).
1088 After UTD or TSHR-CART injection, mice were separated to vehicle control or MAPK inhibitors
1089 (for 2 weeks, for 4 weeks, or continuously until experimental endpoints were reached. **E)** Mice
1090 treated with TSHR-CART cells in combination with MAPK inhibitors showed superior tumor
1091 volume control regardless of the duration of MAPK inhibitor treatment. Tumor volumes were
1092 assessed via caliper measurements in mice treated with UTD or TSHR-CART cells in combination
1093 with vehicle control or MAPK inhibitors (mean and SEM; ns = not significant, *p < 0.05, ****p <
1094 0.0001, two-way ANOVA; n=7 mice per group. **F)** Kaplan-Meier survival curve (**p < 0.01, ***p <
1095 0.001, Log-rank test; n=7 mice per group). **G)** *In vivo* TSHR-CART cell expansion was measured
1096 by absolute count of $hCD45^+$ $hCD3^+$ cells per µL of blood via flow cytometry analysis (mean and
1097 SEM; ns = not significant, one-way ANOVA; n = 7-33 mice per group).

Figure 1

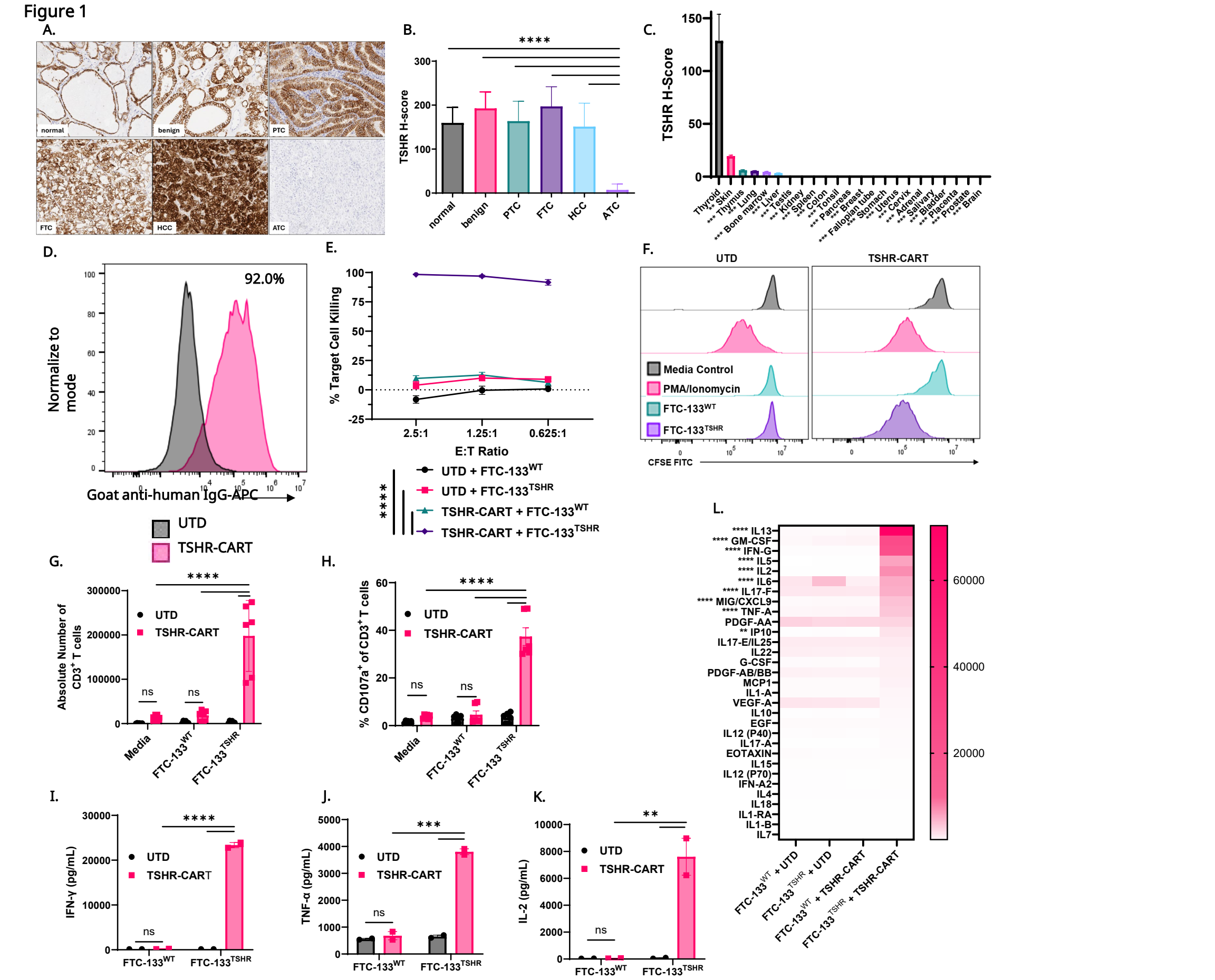
A.
normal
benign
PTC
FTC
HCC
ATC
B.
TSHR H-score
normal
benign
PTC
FTC
HCC
ATC
C.
TSHR H-Score
Thyroid
Skin
Thymus
Lung
Bone marrow
Liver
Testis
Kidney
Spleen
Colon
Tonsil
Pancreas
Breast
Fallopian tube
Stomach
Uterus
Cervix
Adrenal
Salivary
Bladder
Placenta
Prostate
Brain
D.
92.0%
Normalize to mode
Goat anti-human IgG-APC
UTD
TSHR-CART
E.
% Target Cell Killing
2.5:1
1.25:1
0.625:1
E:T Ratio
UTD + FTC-133WT
UTD + FTC-133TSHR
TSHR-CART + FTC-133WT
TSHR-CART + FTC-133TSHR
F.
UTD
TSHR-CART
Media Control
PMA/Ionomycin
FTC-133WT
FTC-133TSHR
CFSE FITC
G.
Absolute Number of CD3+ T cells
UTD
TSHR-CART
ns
Media
FTC-133WT
FTC-133TSHR
H.
% CD107a+ of CD3+ T cells
I.
IFN-γ (pg/mL)
J.
TNF-α (pg/mL)
K.
IL-2 (pg/mL)
L.
IL13
GM-CSF
IFN-G
IL5
IL2
IL6
IL17-F
MIG/CXCL9
TNF-A
PDGF-AA
IP10
IL17-E/IL25
IL22
G-CSF
PDGF-AB/BB
MCP1
IL1-A
VEGF-A
IL10
EGF
IL12 (P40)
IL17-A
EOTAXIN
IL15
IL12 (P70)
IFN-A2
IL4
IL18
IL1-RA
IL1-B
IL7
FTC-133WT + UTD
FTC-133TSHR + UTD
FTC-133WT + TSHR-CART
FTC-133TSHR + TSHR-CART

Figure 2

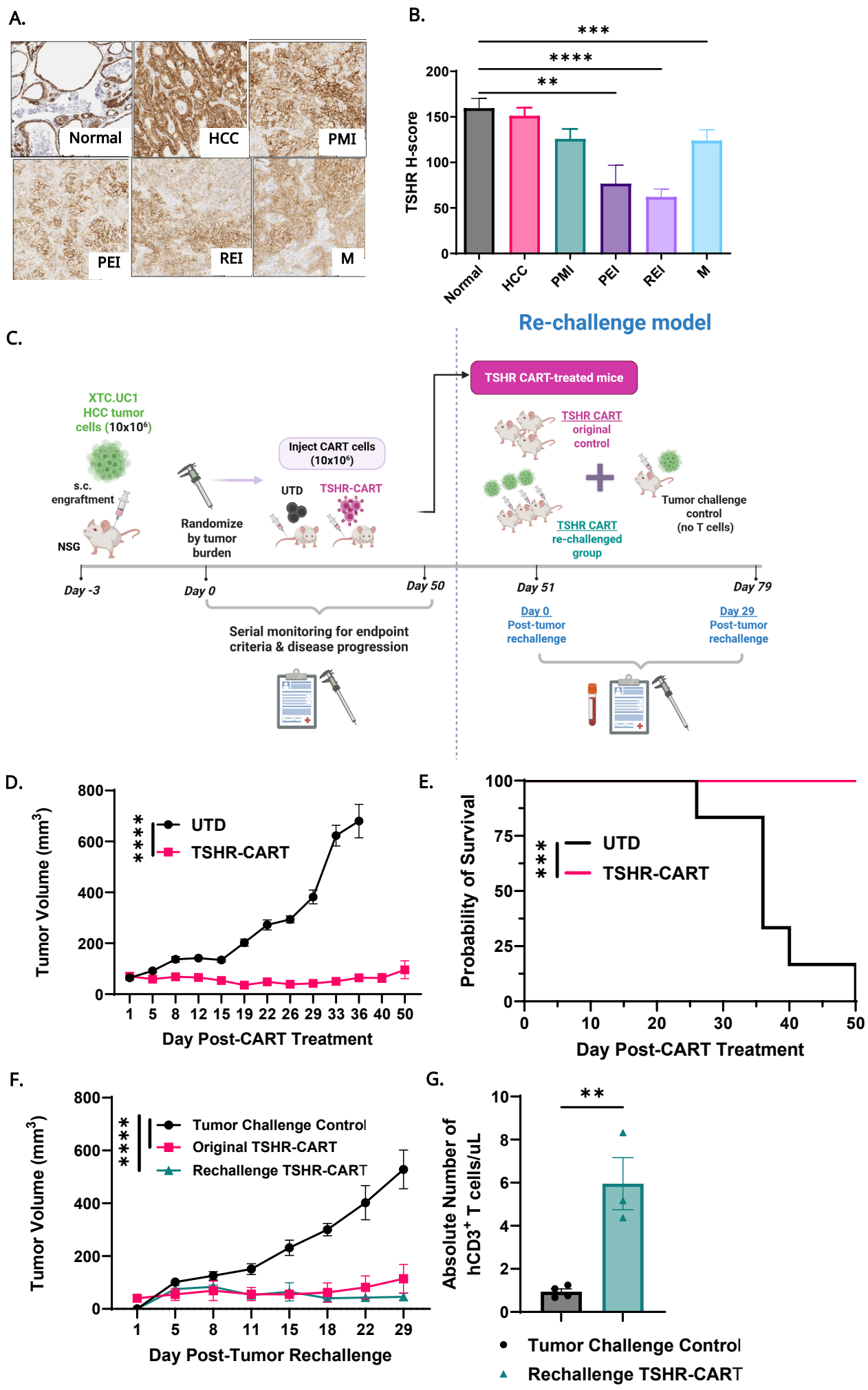
A.
Normal
HCC
PMI
PEI
REI
M
B.
***
****
**
TSHR H-score
200
150
100
50
0
Normal
HCC
PMI
PEI
REI
M
C.
Re-challenge model
XTC.UC1
HCC tumor
cells (10x10⁶)
s.c.
engraftment
NSG
Randomize
by tumor
burden
Inject CART cells
(10x10⁶)
UTD
TSHR-CART
TSHR CART-treated mice
TSHR CART
original
control
TSHR CART
re-challenged
group
Tumor challenge
control
(no T cells)
Day -3
Day 0
Day 50
Day 51
Day 79
Serial monitoring for endpoint
criteria & disease progression
Day 0
Post-tumor
rechallenge
Day 29
Post-tumor
rechallenge
D.
Tumor Volume (mm³)
800
600
400
200
0
****
UTD
TSHR-CART
1 5 8 12 15 19 22 26 29 33 36 40 50
Day Post-CART Treatment
E.
Probability of Survival
100
75
50
25
0
***
UTD
TSHR-CART
0 10 20 30 40 50
Day Post-CART Treatment
F.
Tumor Volume (mm³)
800
600
400
200
0
****
Tumor Challenge Control
Original TSHR-CART
Rechallenge TSHR-CART
1 5 8 11 15 18 22 29
Day Post-Tumor Rechallenge
G.
Absolute Number of
hCD3⁺ T cells/uL
10
8
6
4
2
0
**
Tumor Challenge Control
Rechallenge TSHR-CART

Figure 3

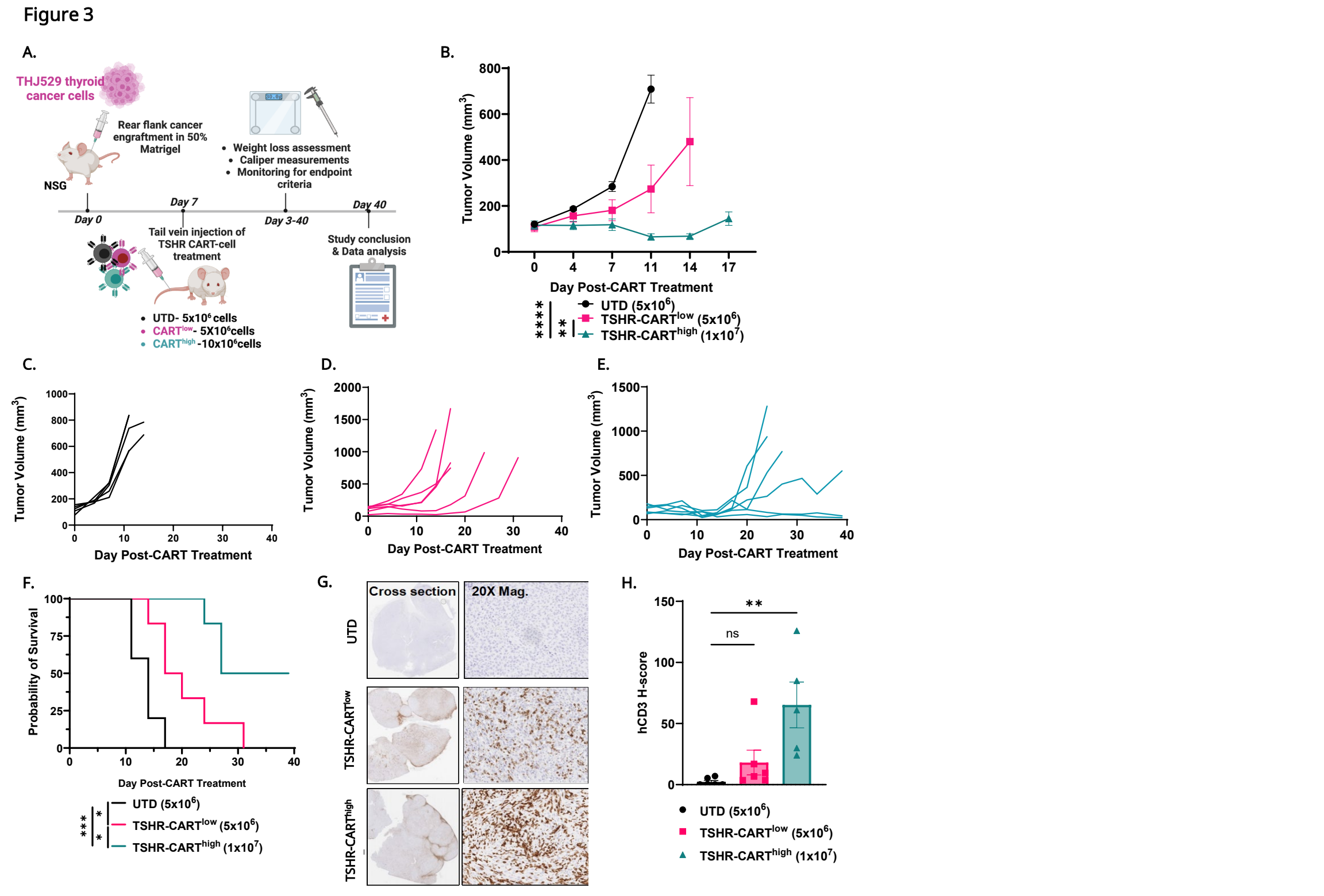
A.
THJ529 thyroid cancer cells
Rear flank cancer engraftment in 50% Matrigel
NSG
Weight loss assessment
Caliper measurements
Monitoring for endpoint criteria
Day 0
Day 7
Day 3-40
Day 40
Tail vein injection of TSHR CART-cell treatment
Study conclusion & Data analysis
UTD- 5x10⁶ cells
CARTlow- 5X10⁶cells
CARThigh -10x10⁶cells
B.
Tumor Volume (mm3)
Day Post-CART Treatment
UTD (5x10⁶)
TSHR-CARTlow (5x10⁶)
TSHR-CARThigh (1x10⁷)
C.
D.
E.
Tumor Volume (mm3)
Day Post-CART Treatment
F.
Probability of Survival
Day Post-CART Treatment
UTD (5x10⁶)
TSHR-CARTlow (5x10⁶)
TSHR-CARThigh (1x10⁷)
G.
Cross section
20X Mag.
UTD
TSHR-CARTlow
TSHR-CARThigh
H.
hCD3 H-score
ns
UTD (5x10⁶)
TSHR-CARTlow (5x10⁶)
TSHR-CARThigh (1x10⁷)

Figure 4

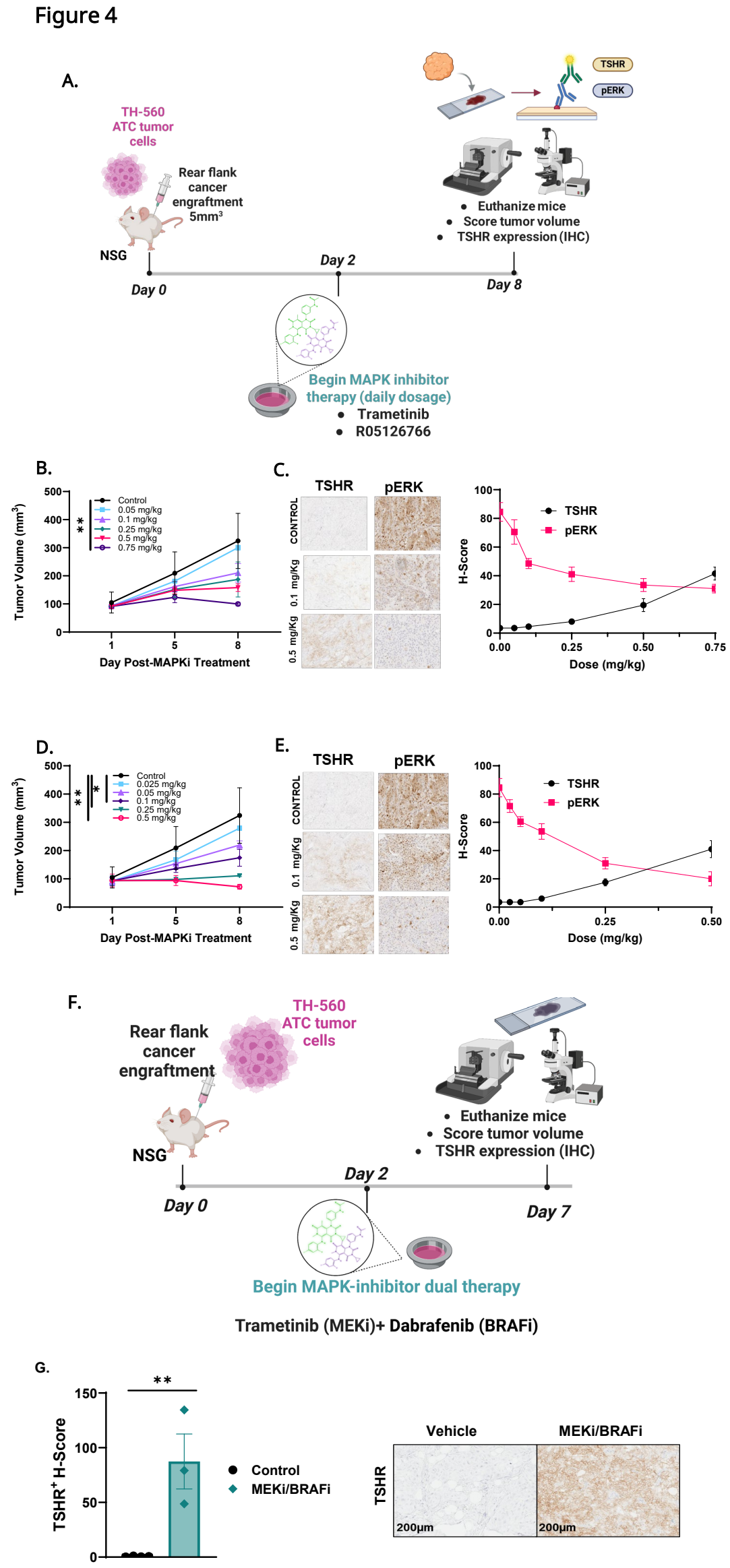
A.
TH-560
ATC tumor
cells
Rear flank
cancer
engraftment
5mm³
NSG
Day 0
Day 2
Day 8
TSHR
pERK
Euthanize mice
Score tumor volume
TSHR expression (IHC)
Begin MAPK inhibitor
therapy (daily dosage)
Trametinib
R05126766
B.
Tumor Volume (mm³)
Control
0.05 mg/kg
0.1 mg/kg
0.25 mg/kg
0.5 mg/kg
0.75 mg/kg
Day Post-MAPKi Treatment
C.
TSHR
pERK
CONTROL
0.1 mg/Kg
0.5 mg/Kg
H-Score
Dose (mg/kg)
D.
Tumor Volume (mm³)
Control
0.025 mg/kg
0.05 mg/kg
0.1 mg/kg
0.25 mg/kg
0.5 mg/kg
Day Post-MAPKi Treatment
E.
TSHR
pERK
CONTROL
0.1 mg/Kg
0.5 mg/Kg
H-Score
Dose (mg/kg)

F.
Rear flank
cancer
engraftment
TH-560
ATC tumor
cells
NSG
Euthanize mice
Score tumor volume
TSHR expression (IHC)
Day 0
Day 2
Day 7
Begin MAPK-inhibitor dual therapy
Trametinib (MEKi)+ Dabrafenib (BRAFi)
G.
TSHR⁺ H-Score
Control
MEKi/BRAFi
Vehicle
MEKi/BRAFi
TSHR
200µm
200µm

Figure 5

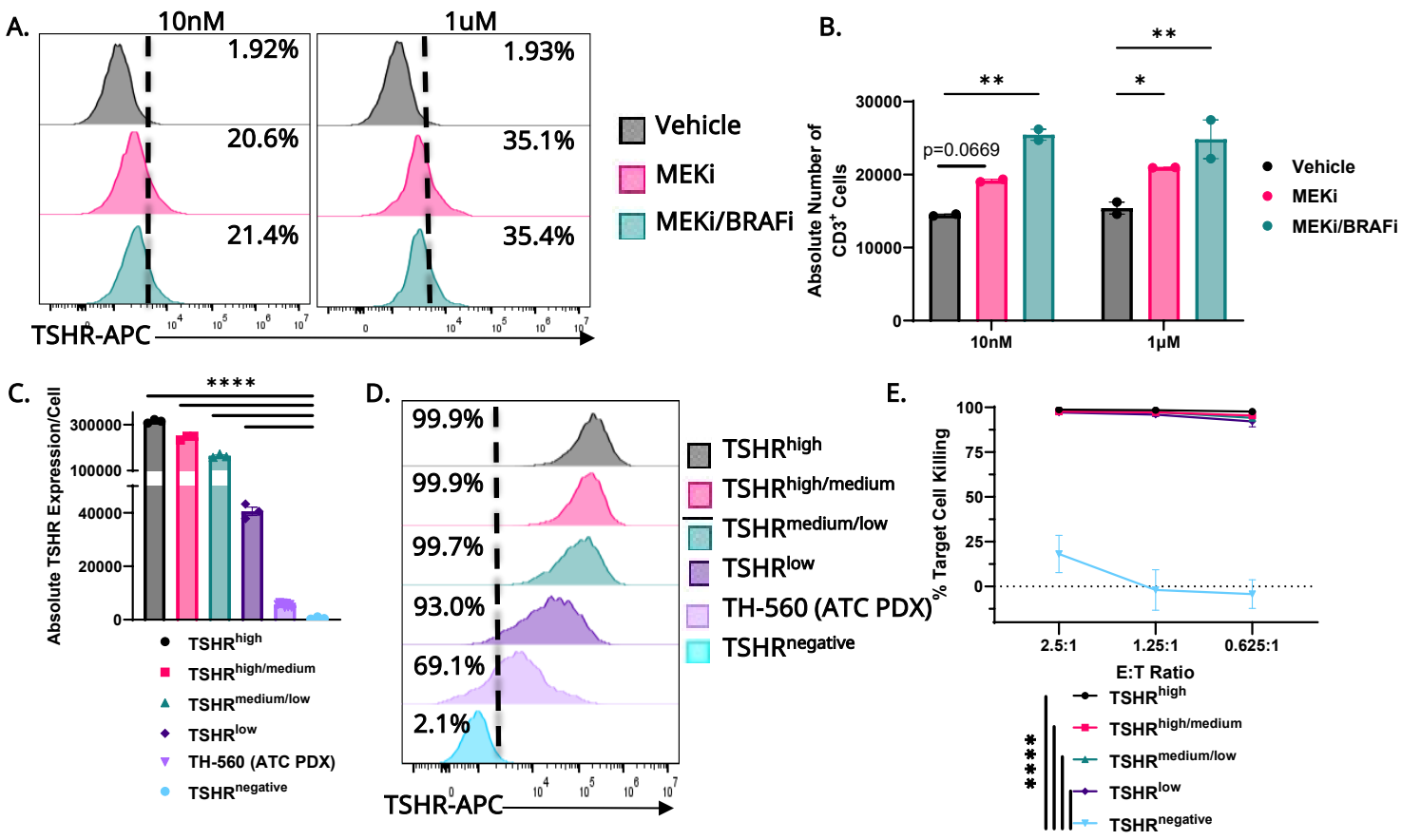
A.
10nM
1uM
1.92%
20.6%
21.4%
1.93%
35.1%
35.4%
TSHR-APC
Vehicle
MEKi
MEKi/BRAFi
B.
Absolute Number of CD3+ Cells
p=0.0669
10nM
1μM
Vehicle
MEKi
MEKi/BRAFi
C.
Absolute TSHR Expression/Cell
TSHRhigh
TSHRhigh/medium
TSHRmedium/low
TSHRlow
TH-560 (ATC PDX)
TSHRnegative
D.
99.9%
99.9%
99.7%
93.0%
69.1%
2.1%
TSHR-APC
TSHRhigh
TSHRhigh/medium
TSHRmedium/low
TSHRlow
TH-560 (ATC PDX)
TSHRnegative
E.
% Target Cell Killing
2.5:1
1.25:1
0.625:1
E:T Ratio
TSHRhigh
TSHRhigh/medium
TSHRmedium/low
TSHRlow
TSHRnegative

Figure 6

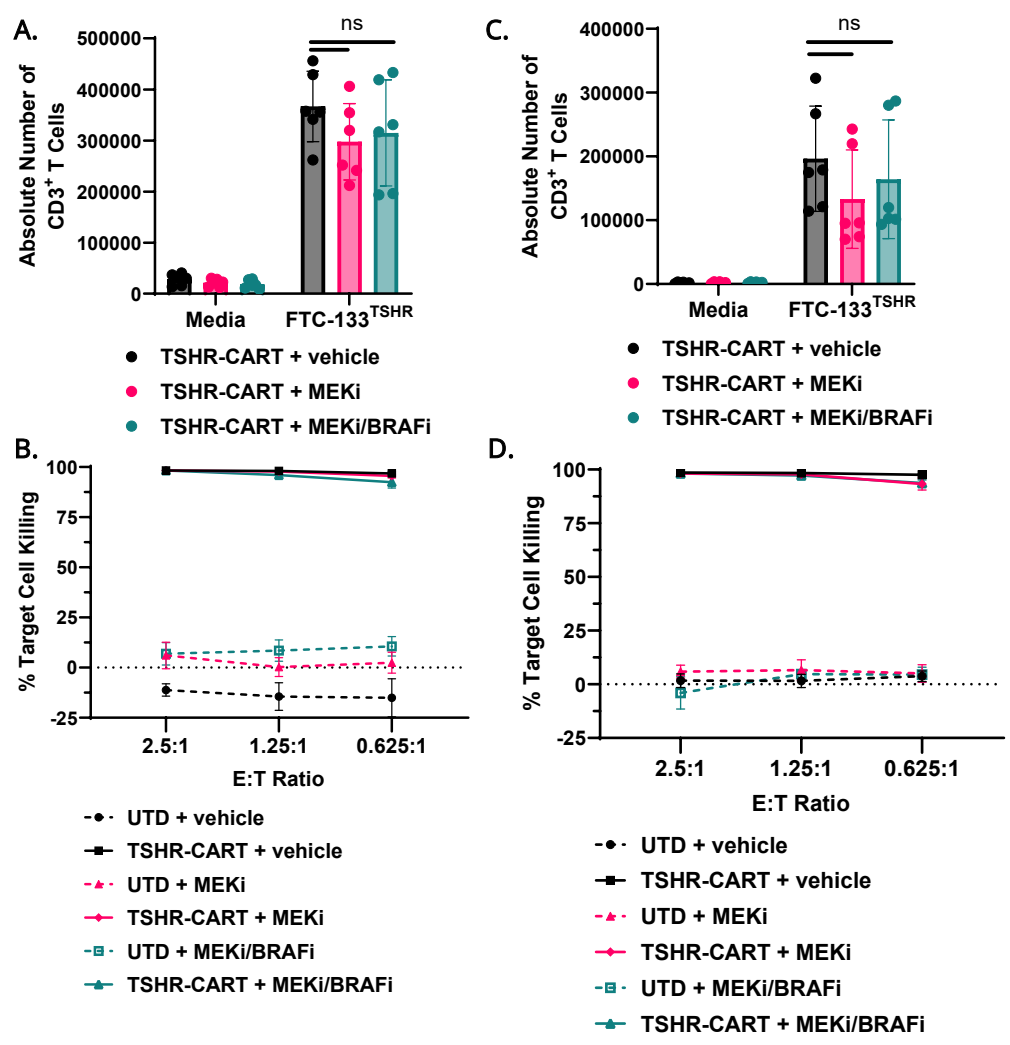
A.
ns
Absolute Number of CD3+ T Cells
500000
400000
300000
200000
100000
0
Media
FTC-133TSHR
TSHR-CART + vehicle
TSHR-CART + MEKi
TSHR-CART + MEKi/BRAFi
C.
ns
Absolute Number of CD3+ T Cells
400000
300000
200000
100000
0
Media
FTC-133TSHR
TSHR-CART + vehicle
TSHR-CART + MEKi
TSHR-CART + MEKi/BRAFi
B.
% Target Cell Killing
100
75
50
25
0
-25
2.5:1
1.25:1
0.625:1
E:T Ratio
UTD + vehicle
TSHR-CART + vehicle
UTD + MEKi
TSHR-CART + MEKi
UTD + MEKi/BRAFi
TSHR-CART + MEKi/BRAFi
D.
% Target Cell Killing
100
75
50
25
0
-25
2.5:1
1.25:1
0.625:1
E:T Ratio
UTD + vehicle
TSHR-CART + vehicle
UTD + MEKi
TSHR-CART + MEKi
UTD + MEKi/BRAFi
TSHR-CART + MEKi/BRAFi

Figure 7

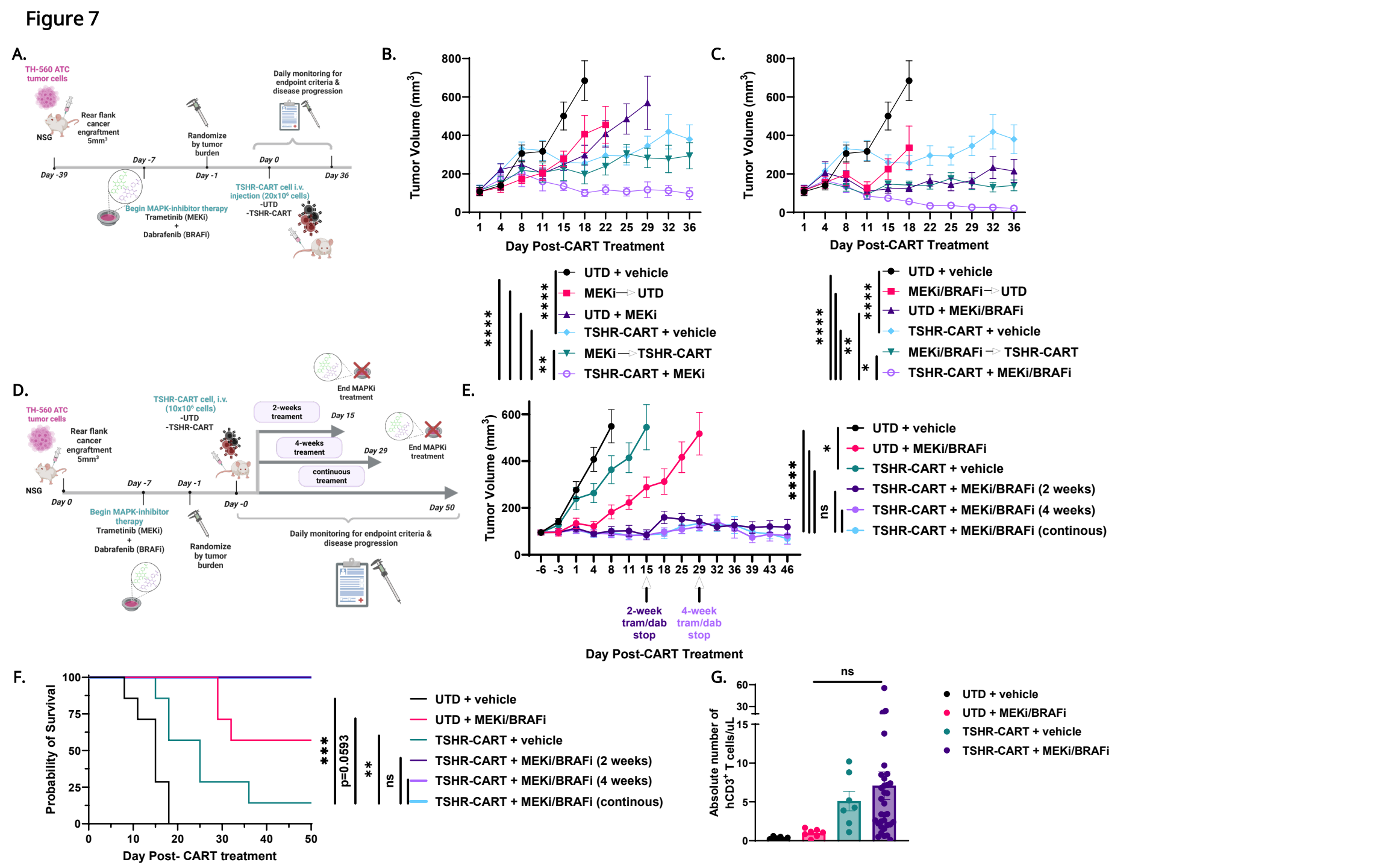
A.
TH-560 ATC tumor cells
NSG
Rear flank cancer engraftment 5mm³
Randomize by tumor burden
Daily monitoring for endpoint criteria & disease progression
Day -39
Day -7
Day -1
Day 0
Day 36
Begin MAPK-inhibitor therapy
Trametinib (MEKi)
+
Dabrafenib (BRAFi)
TSHR-CART cell i.v. injection (20x10⁶ cells)
-UTD
-TSHR-CART
B.
Tumor Volume (mm³)
Day Post-CART Treatment
UTD + vehicle
MEKi → UTD
UTD + MEKi
TSHR-CART + vehicle
MEKi → TSHR-CART
TSHR-CART + MEKi
C.
Tumor Volume (mm³)
Day Post-CART Treatment
UTD + vehicle
MEKi/BRAFi → UTD
UTD + MEKi/BRAFi
TSHR-CART + vehicle
MEKi/BRAFi → TSHR-CART
TSHR-CART + MEKi/BRAFi
D.
TH-560 ATC tumor cells
NSG
Rear flank cancer engraftment 5mm³
TSHR-CART cell, i.v. (10x10⁶ cells)
-UTD
-TSHR-CART
2-weeks treament
4-weeks treament
continuous treament
Day 15
Day 29
Day 50
End MAPKi treatment
Day 0
Day -7
Day -1
Day -0
Begin MAPK-inhibitor therapy
Trametinib (MEKi)
+
Dabrafenib (BRAFi)
Randomize by tumor burden
Daily monitoring for endpoint criteria & disease progression
E.
Tumor Volume (mm³)
UTD + vehicle
UTD + MEKi/BRAFi
TSHR-CART + vehicle
TSHR-CART + MEKi/BRAFi (2 weeks)
TSHR-CART + MEKi/BRAFi (4 weeks)
TSHR-CART + MEKi/BRAFi (continous)
ns
2-week tram/dab stop
4-week tram/dab stop
Day Post-CART Treatment
F.
Probability of Survival
Day Post- CART treatment
p=0.0593
ns
UTD + vehicle
UTD + MEKi/BRAFi
TSHR-CART + vehicle
TSHR-CART + MEKi/BRAFi (2 weeks)
TSHR-CART + MEKi/BRAFi (4 weeks)
TSHR-CART + MEKi/BRAFi (continous)
G.
ns
Absolute number of hCD3⁺ T cells/uL
UTD + vehicle
UTD + MEKi/BRAFi
TSHR-CART + vehicle
TSHR-CART + MEKi/BRAFi

Sup. Fig. S1

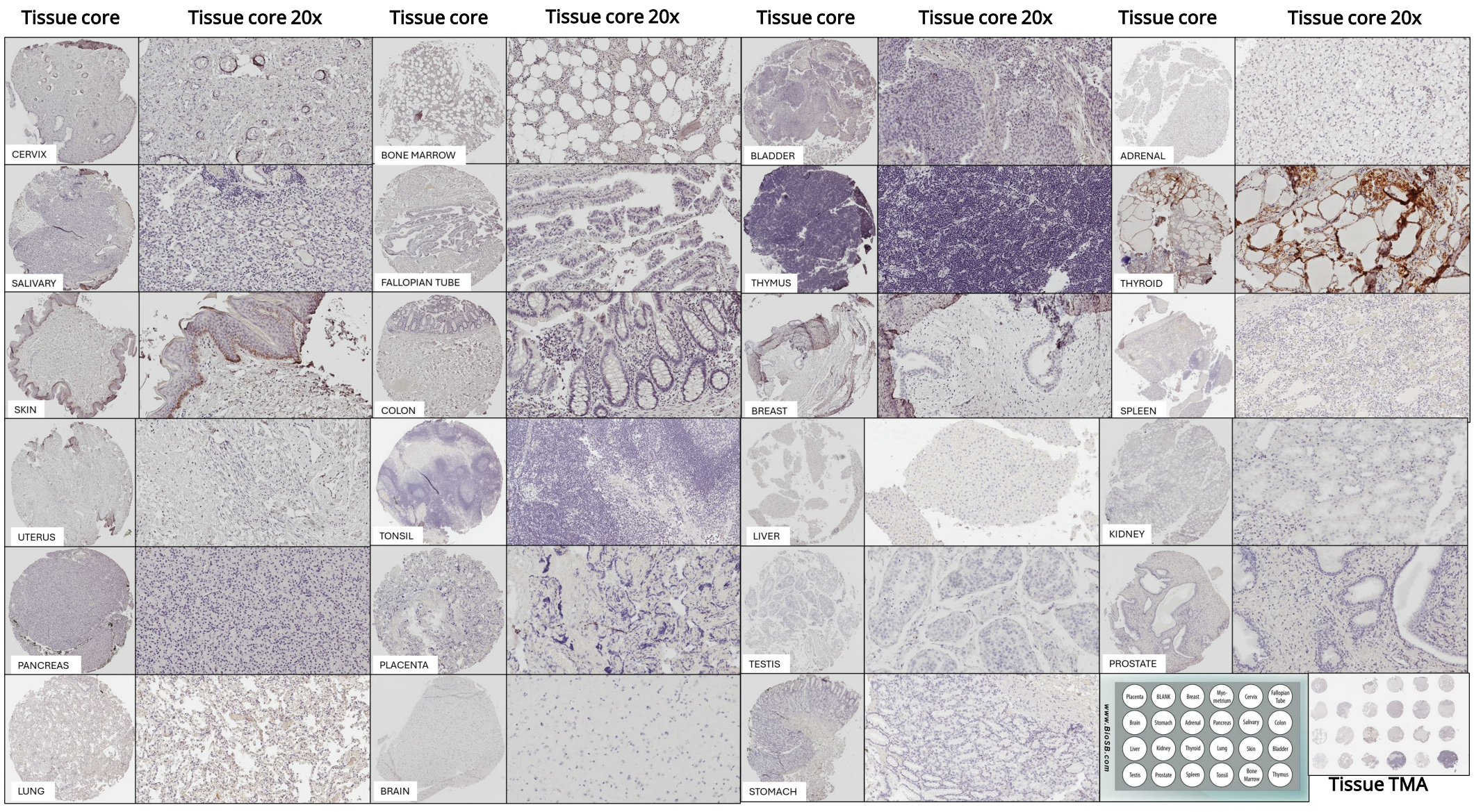
Tissue core
Tissue core 20x
Tissue core
Tissue core 20x
Tissue core
Tissue core 20x
Tissue core
Tissue core 20x
CERVIX
BONE MARROW
BLADDER
ADRENAL
SALIVARY
FALLOPIAN TUBE
THYMUS
THYROID
SKIN
COLON
BREAST
SPLEEN
UTERUS
TONSIL
LIVER
KIDNEY
PANCREAS
PLACENTA
TESTIS
PROSTATE
LUNG
BRAIN
STOMACH
www.BioSB.com
Placenta
BLANK
Breast
Myo-metrium
Cervix
Fallopian Tube
Brain
Stomach
Adrenal
Pancreas
Salivary
Colon
Liver
Kidney
Thyroid
Lung
Skin
Bladder
Testis
Prostate
Spleen
Tonsil
Bone Marrow
Thymus
Tissue TMA

Sup. Fig. S2

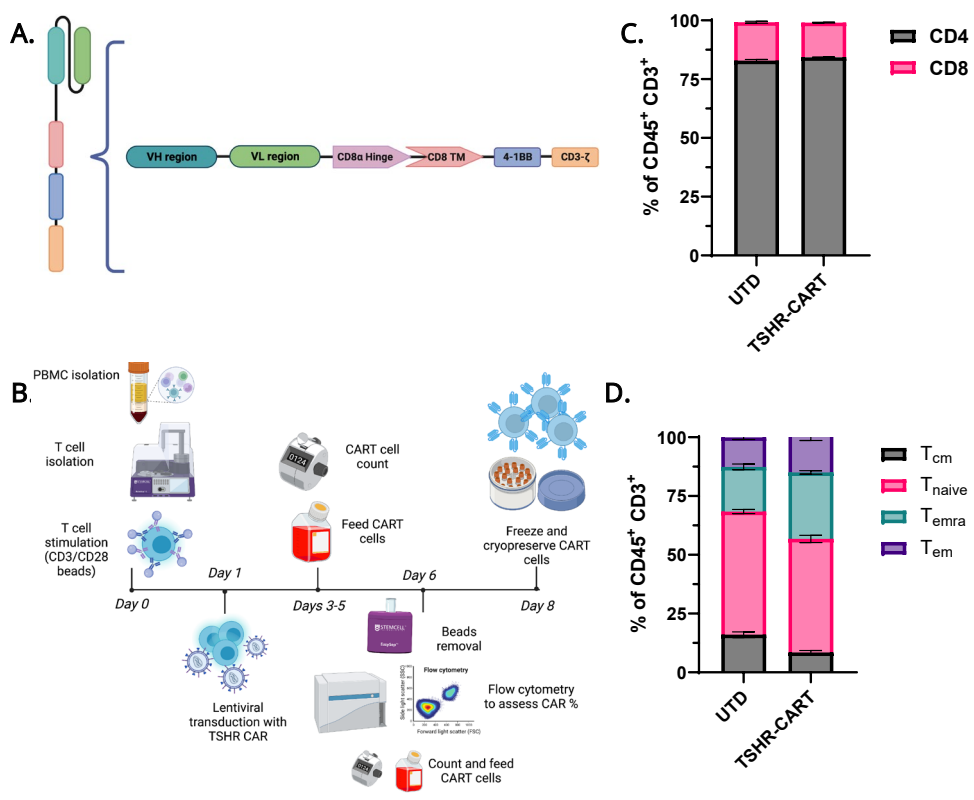
A.
VH region
VL region
CD8α Hinge
CD8 TM
4-1BB
CD3-ζ
B.
PBMC isolation
T cell isolation
T cell stimulation (CD3/CD28 beads)
CART cell count
Feed CART cells
Freeze and cryopreserve CART cells
Day 0
Day 1
Days 3-5
Day 6
Day 8
Beads removal
Lentiviral transduction with TSHR CAR
Flow cytometry to assess CAR %
Count and feed CART cells
C.
% of CD45+ CD3+
100
75
50
25
0
UTD
TSHR-CART
CD4
CD8
D.
% of CD45+ CD3+
100
75
50
25
0
UTD
TSHR-CART
Tcm
Tnaive
Temra
Tem

Sup. Fig. S3

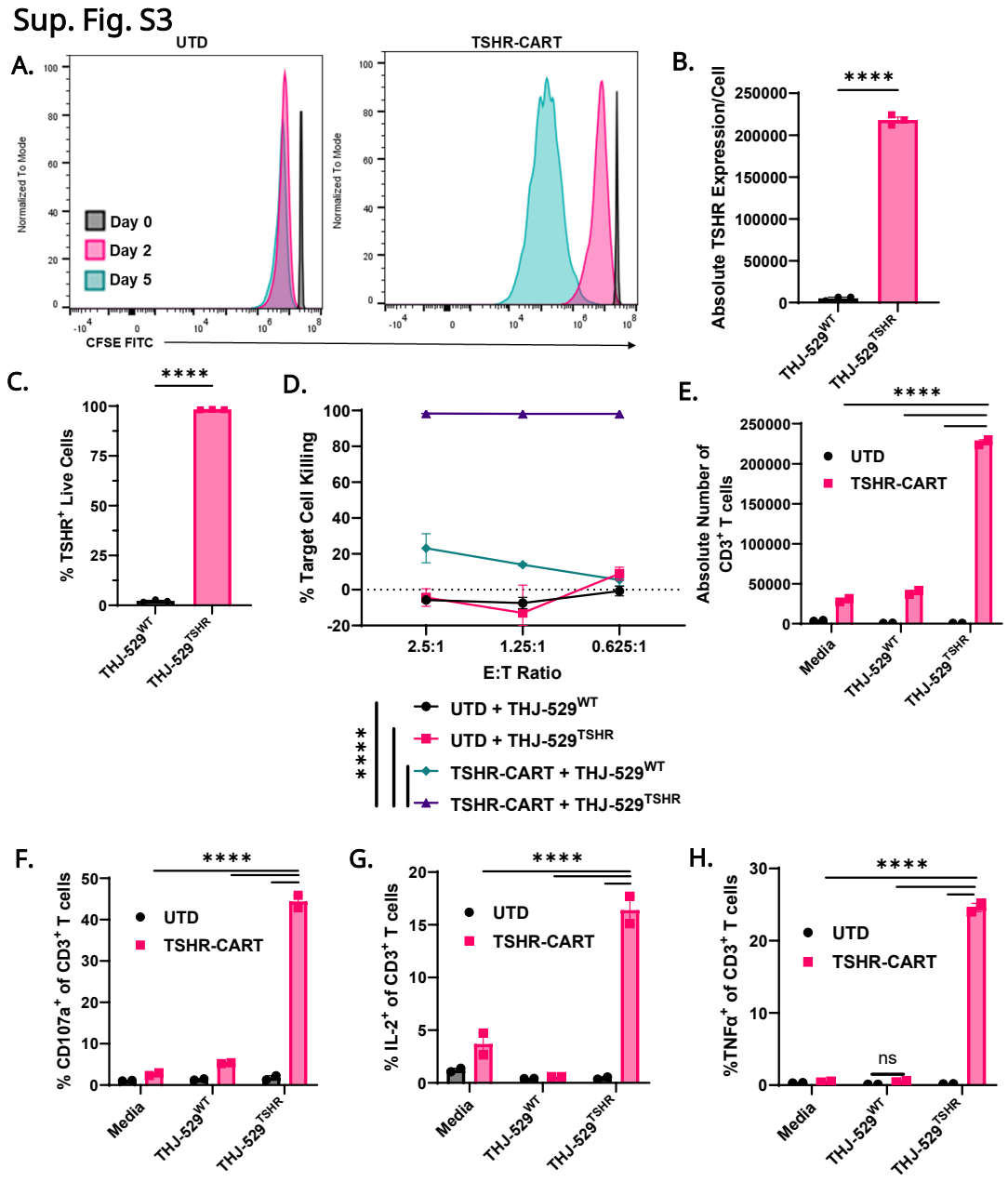
A.
UTD
TSHR-CART
Normalized To Mode
Day 0
Day 2
Day 5
CFSE FITC
B.
Absolute TSHR Expression/Cell
****
THJ-529WT
THJ-529TSHR
C.
% TSHR+ Live Cells
****
D.
% Target Cell Killing
E:T Ratio
2.5:1
1.25:1
0.625:1
UTD + THJ-529WT
UTD + THJ-529TSHR
TSHR-CART + THJ-529WT
TSHR-CART + THJ-529TSHR
E.
Absolute Number of CD3+ T cells
UTD
TSHR-CART
Media
F.
% CD107a+ of CD3+ T cells
G.
% IL-2+ of CD3+ T cells
H.
%TNFα+ of CD3+ T cells
ns

Sup. Fig. S4

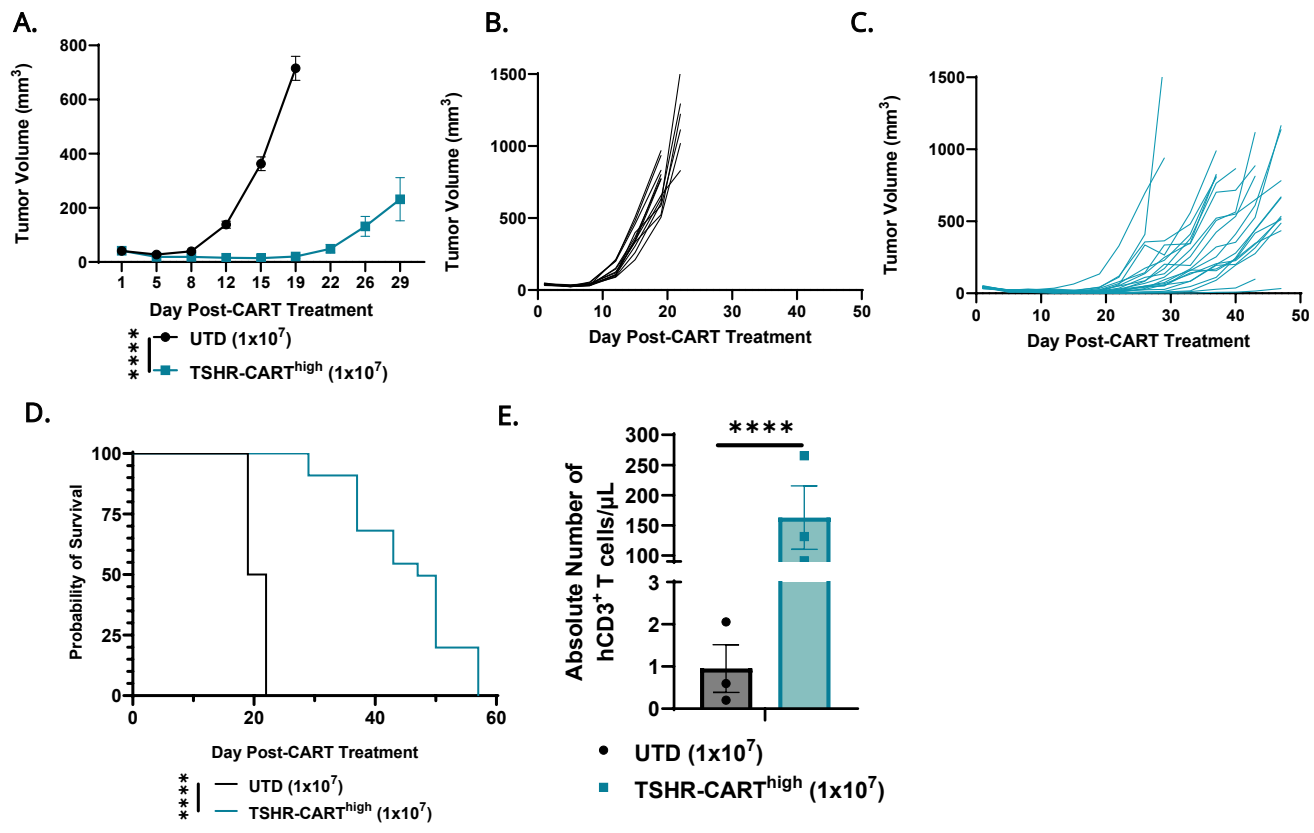
A.
Tumor Volume (mm3)
Day Post-CART Treatment
UTD (1x107)
TSHR-CARThigh (1x107)
B.
Tumor Volume (mm3)
Day Post-CART Treatment
C.
Tumor Volume (mm3)
Day Post-CART Treatment
D.
Probability of Survival
Day Post-CART Treatment
UTD (1x107)
TSHR-CARThigh (1x107)
E.
Absolute Number of hCD3+ T cells/µL
****
UTD (1x107)
TSHR-CARThigh (1x107)

Sup. Fig. S5

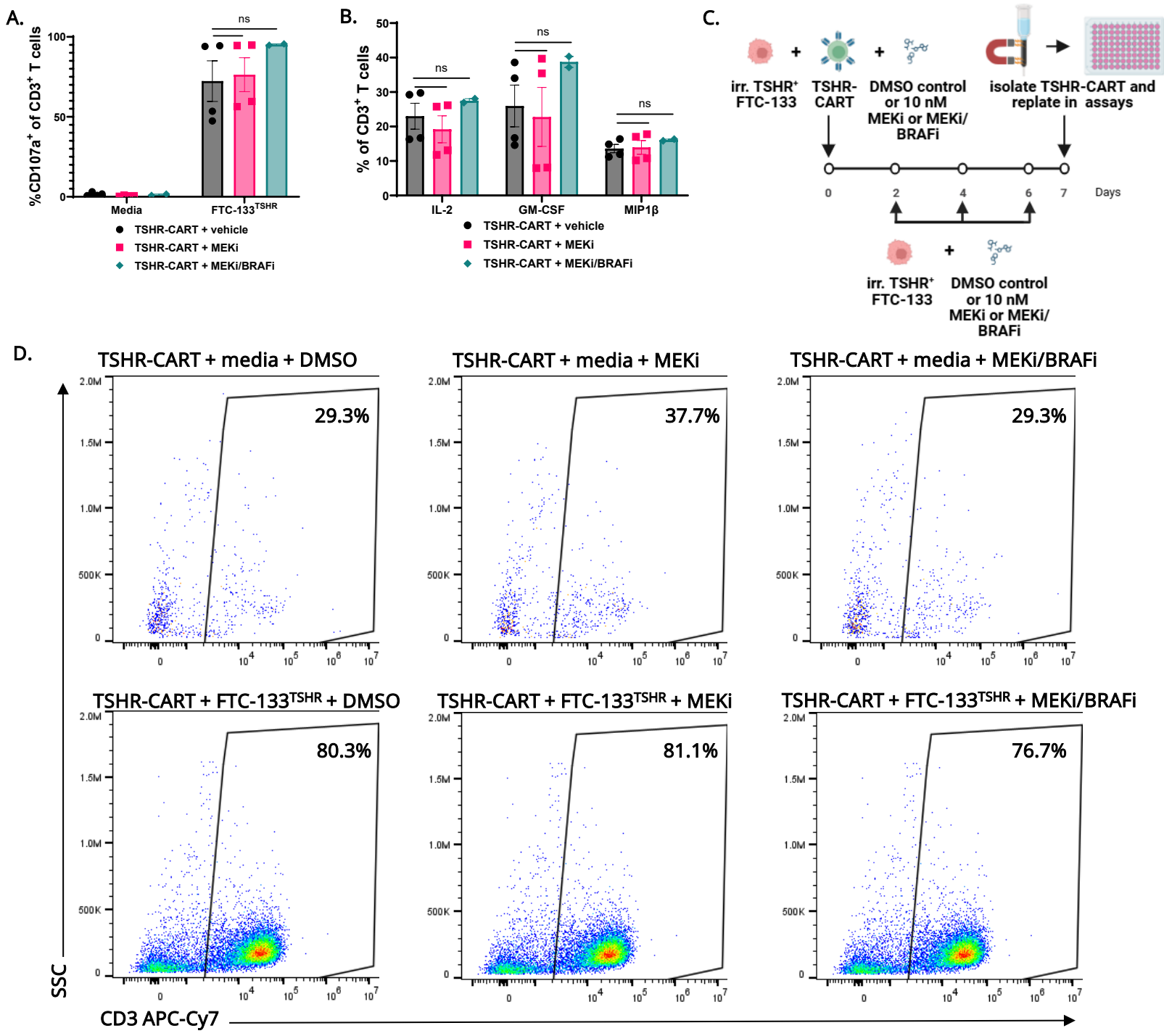
A.
%CD107a+ of CD3+ T cells
ns
Media
FTC-133TSHR
TSHR-CART + vehicle
TSHR-CART + MEKi
TSHR-CART + MEKi/BRAFi
B.
% of CD3+ T cells
IL-2
GM-CSF
MIP1β
C.
irr. TSHR+ FTC-133
TSHR-CART
DMSO control or 10 nM MEKi or MEKi/BRAFi
isolate TSHR-CART and replate in assays
Days
D.
TSHR-CART + media + DMSO
29.3%
TSHR-CART + media + MEKi
37.7%
TSHR-CART + media + MEKi/BRAFi
29.3%
TSHR-CART + FTC-133TSHR + DMSO
80.3%
TSHR-CART + FTC-133TSHR + MEKi
81.1%
TSHR-CART + FTC-133TSHR + MEKi/BRAFi
76.7%
SSC
CD3 APC-Cy7

Sup. Fig. S6

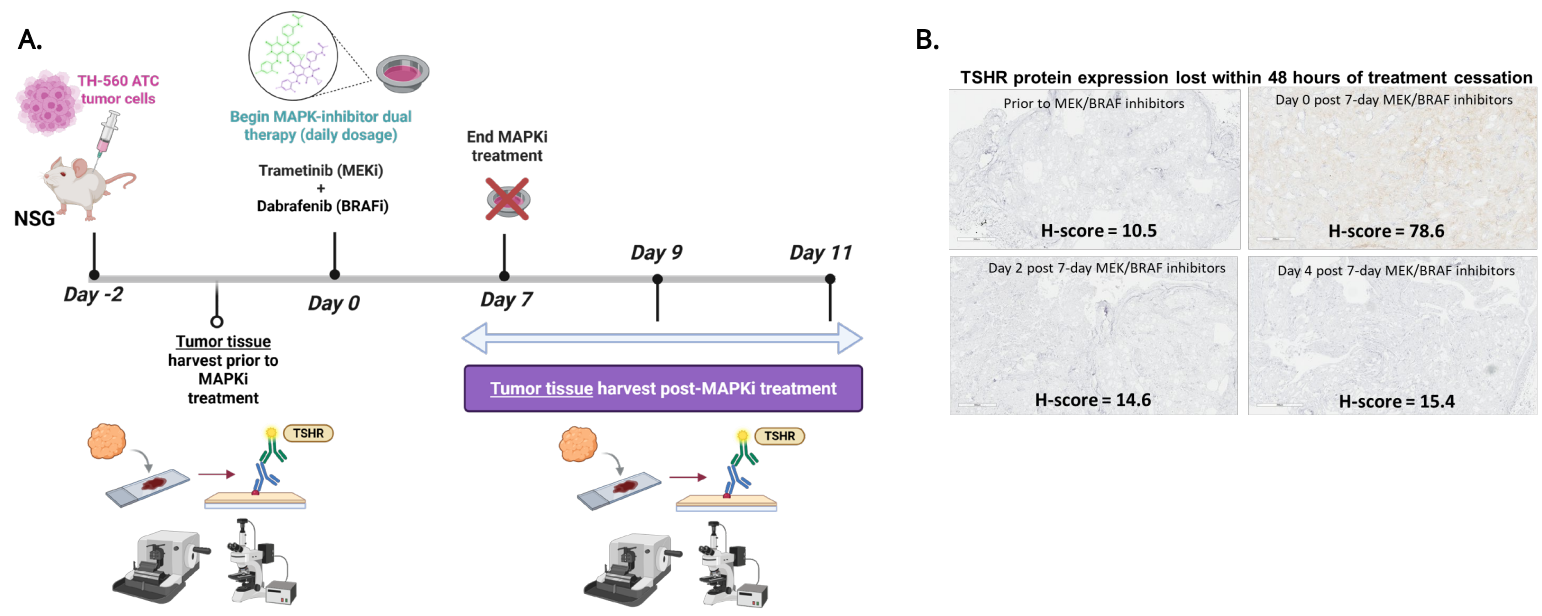
A.
TH-560 ATC tumor cells
NSG
Begin MAPK-inhibitor dual therapy (daily dosage)
Trametinib (MEKi)
+
Dabrafenib (BRAFi)
End MAPKi treatment
Day -2
Day 0
Day 7
Day 9
Day 11
Tumor tissue harvest prior to MAPKi treatment
Tumor tissue harvest post-MAPKi treatment
TSHR
TSHR
B.
TSHR protein expression lost within 48 hours of treatment cessation
Prior to MEK/BRAF inhibitors
H-score = 10.5
Day 0 post 7-day MEK/BRAF inhibitors
H-score = 78.6
Day 2 post 7-day MEK/BRAF inhibitors
H-score = 14.6
Day 4 post 7-day MEK/BRAF inhibitors
H-score = 15.4

Sup. Fig. S7

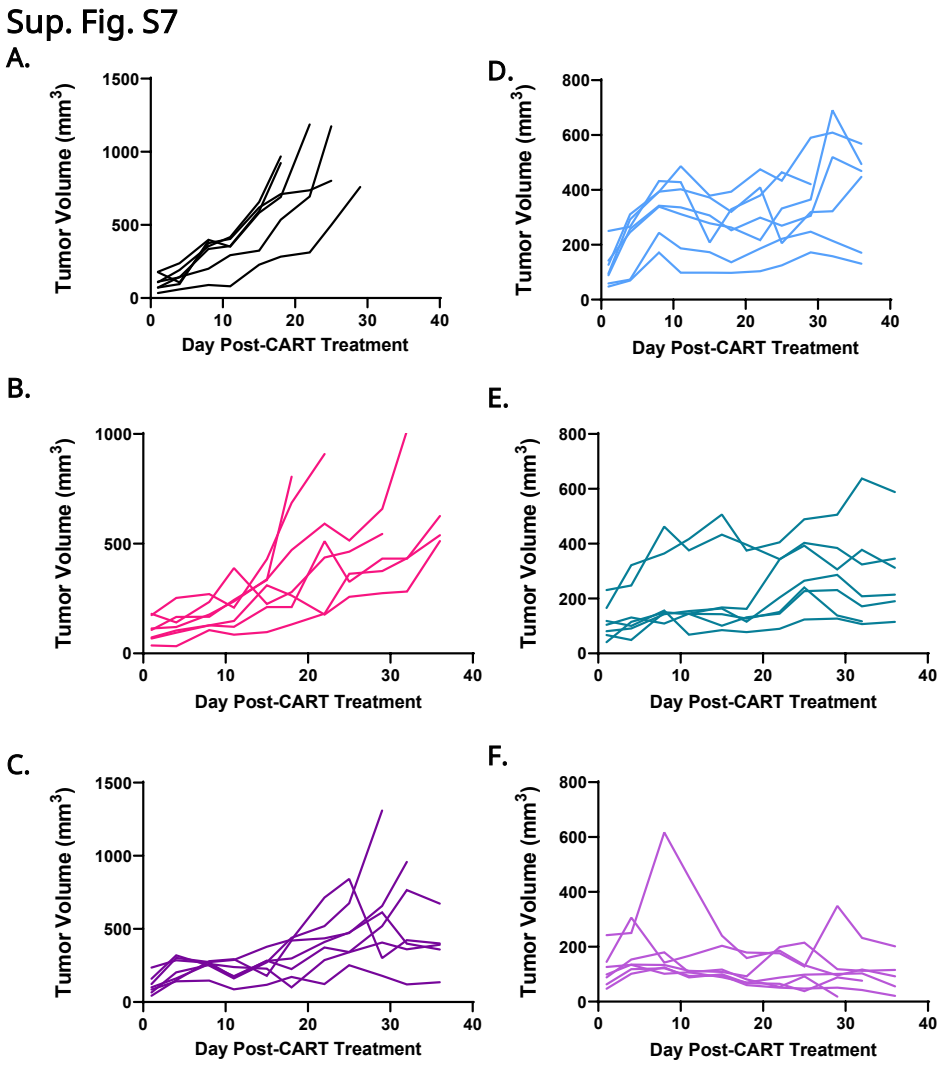

Sup. Fig. S8

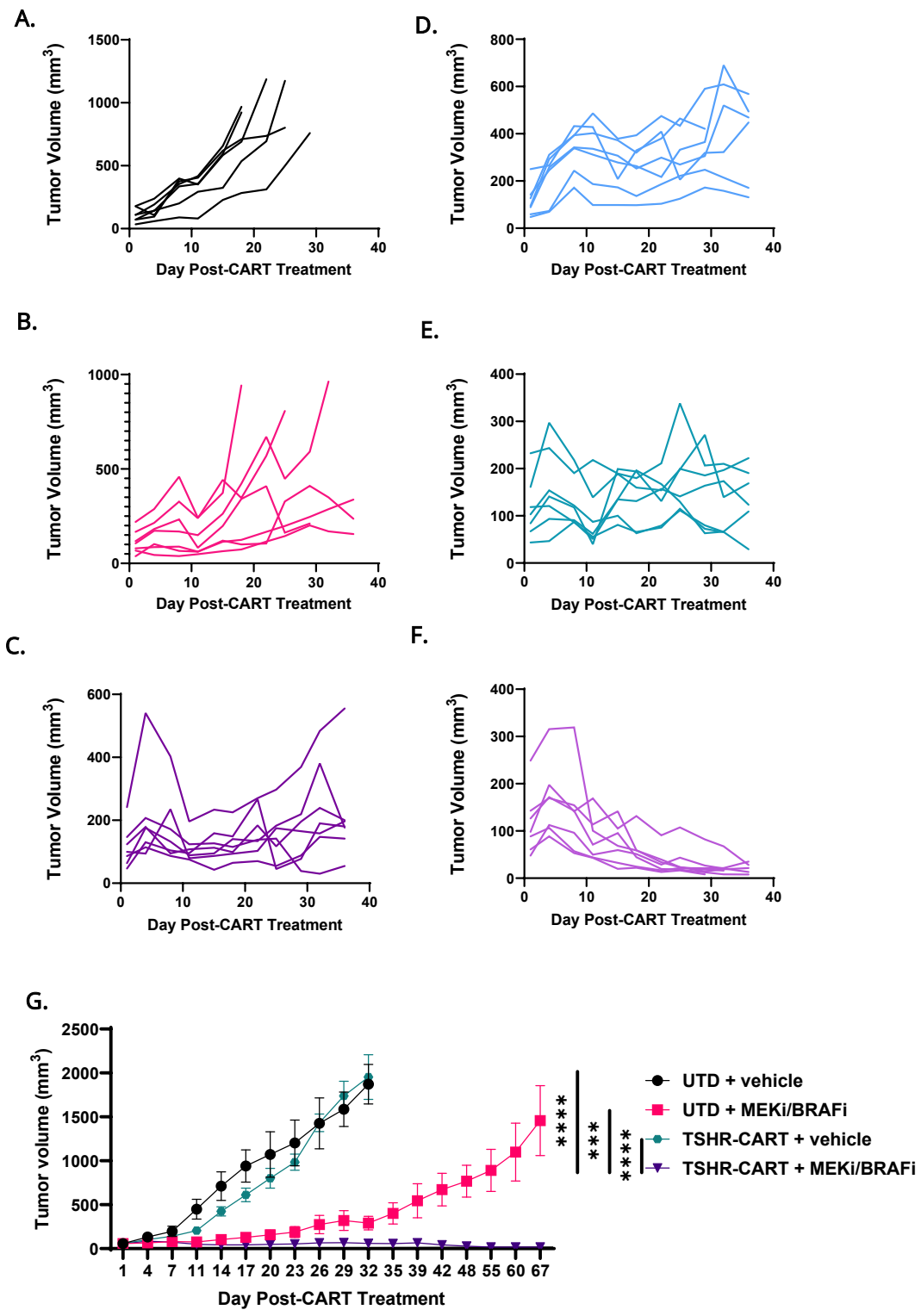
A.
B.
C.
D.
E.
F.
G.
Tumor Volume (mm3)
Day Post-CART Treatment
Tumor volume (mm3)
UTD + vehicle
UTD + MEKi/BRAFi
TSHR-CART + vehicle
TSHR-CART + MEKi/BRAFi
****
***
****

Sup. Fig. S9

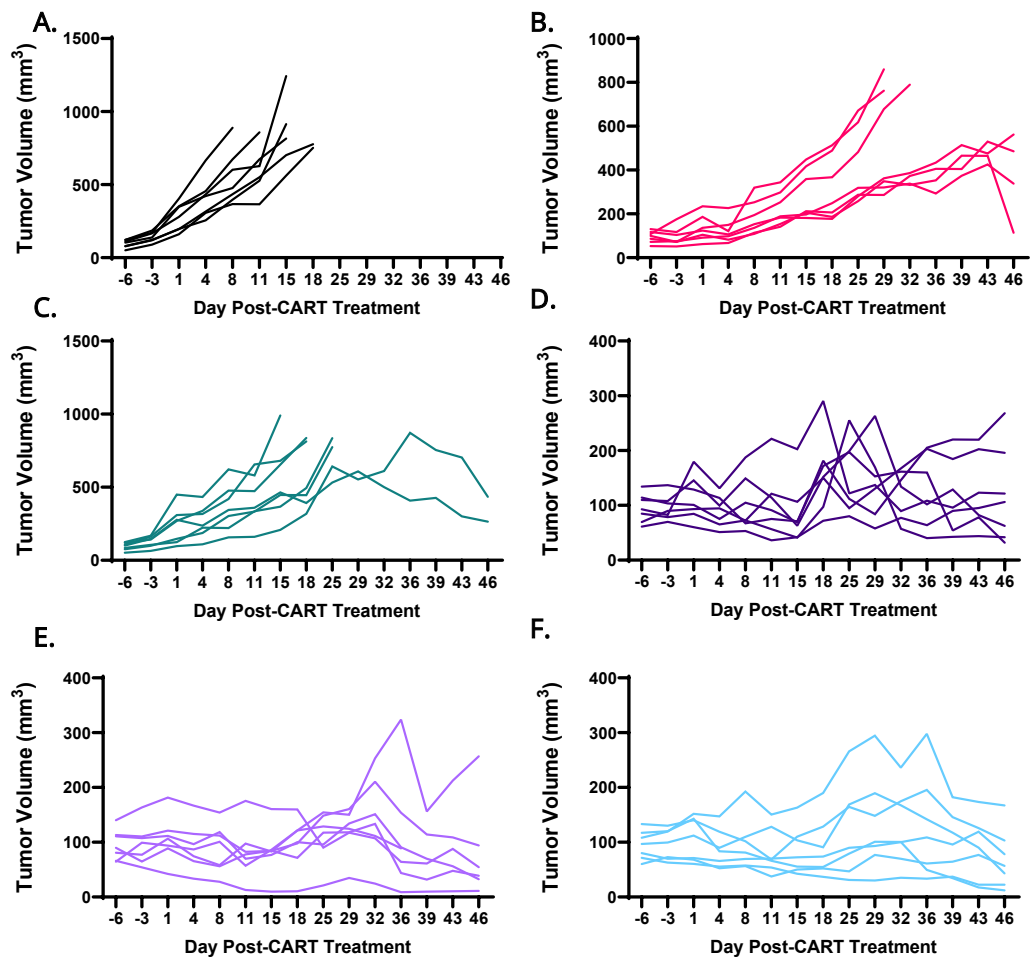
A.
B.
C.
D.
E.
F.
Tumor Volume (mm3)
Day Post-CART Treatment
-6 -3 1 4 8 11 15 18 25 29 32 36 39 43 46